

Dear Roger Soliva,

Please find below again our response to the reviewers, this time with the respected line numbers corresponding to the markup version of the revised manuscript, which is also attached below. We fully understand that without line numbers an evaluation of the revised manuscript was difficult. Also, in red color, we added additional clarifications to the response.

With respect to your note on the need of more explanations in results and discussion, more/better details on the petrography, etc., we think that this is what we have covered in our revisions.

You suggest to use the IGV for estimating the burial depth of the sandstone / formation depth of the calcite cement, which is indeed a tempting approach. However, we see two major problems in such an assessment: First, the compaction curve of Paxton et al (2002) is based on mature, well rounded sandstone, which is very different from the sandstone analyzed here, i.e. poorly sorted, angular to subangular grains, and a significant amount of “ductile” framework grains like biotite. Second, there is a huge scatter in IGV data at any given burial depth (e.g., see compilation of Taylor et al., 2010, AAPG Bull). Hence, without running a proper compaction modeling, which is beyond the scope of this contribution, the use of IGV would not hold sustainable insights for narrowing down the formation depth of the calcite cement.

Kind regards,

Eric Salomon

on behalf of all authors of this contribution

Author response to comments of Reviewer 1 on “Fault-controlled fluid circulation and diagenesis along basin bounding fault systems in rifts – insights from the East Greenland rift system” by Salomon et al. (response indented and in italic)

This is a well written and illustrated paper that is worthy of publication. It nicely documents how early diagenetic, fault-controlled cementation can modify rock physical properties and thereby control subsequent fracture patterns, fluid flow and diagenetic overprint. I would recommend moderate revisions prior to publication in order to clarify a few points, and in particular to expand a little more on the conceptual model that is presented. In particular, Figs 10 and 11 are very well drawn but need a lot more explanation in the text. I really couldn't see why Fig 10 was needed – Fig. 11 works very well and is specific to the study area. However, in order to build up the rationale for the conceptual model a number of issues need to be more fully explained:

Use of figure 10: We decided to include this figure, because we thought without showing the general subsurface flow pattern in coastal areas, it would be difficult to understand the suggested flow lines of marine subsurface water in figure 11 (e.g., to avoid the question of why the flow lines are not the other way around.).

More explanations to model: We think that this is covered with the overall revisions, i.e. the improved discussion on the stable isotope data, minor element data, and on permeability of the cementation zone.

1. There needs to be a clear definition early in the paper as to what is meant by 'early syn-rift', 'rift climax', 'post-rift', etc. and ideally these timings should be shown on Fig. 1b and briefly described in the text. I got a bit confused in parts of the paper as to the actual timing that was being discussed.

We added the timings to the stratigraphy column in Fig. 1b and in the text it is now clarified that such a subdivision is made. We also clarify that “early syn rift” is broadly similar to rift initiation (sensu Prosser, 1993). [lines 103-105]

2. The discussion as to how quickly cementation occurred (~lines 270 – 275) needs to be drawn out a little more as the prose jumps around a bit. Establish that the most reliable dates for matrix cementation are ~150 to 140Ma, then give the age of the LB Formation. From there, build the argument of increased tensile strength controlling fracturing and use the date of G-10v1 as evidence that matrix cementation happened immediately post-deposition. This is the core of your paper, so needs to be carefully explained.

We remodelled this section by shifting the vein age of G-10 v1 in front of the discussion of recrystallization of the younger cement ages to clarify the age boundary of the cementation zone. [lines 328-343]

3. Figure 9 uses an interpolation of dip to calculate depth of cementation based on the present day erosional profile, but I am not totally convinced by this because:
 - there is no mention of structural tilt, which must have occurred as a result of uplift and doming in the Cenozoic?
 - The estimation of 10 or 15° depositional dip seems steep and I couldn't find reference earlier in the paper (e.g. from field measurements) as to where this value might have come from. Maybe I missed it. However, given that a 5° dip difference (from 10 to 15°)

has an impact of ~300 m change in burial depth, should a lower dip (e.g. 6°?) also be shown?

- The effect of compaction is referred to in brackets, yet this is important. Thickness is estimated from interpolation/extrapolation from ~4km from the fault, but at >1km from the fault there would have been more compaction than within the cemented zone, which presumably is undercompacted because of the effect of early cementation. What do you know of compaction from petrographical analysis of uncemented sandstones?

The reviewer raises valid points here, which are difficult to address though, as this implies a lot of speculation:

- Compaction: The reviewer is right, that the calcite-cemented fault-promixal sediments are less compacted than the uncemented fault-distal sediments. From a rough image analysis this amounts to ~35 % vs ~20% intergranular volume. However, for a proper compaction analysis it would be necessary to know the thickness of the Lindemans Bugt Formation and the early syn-rift sediments (comprising significant amounts of clay) underneath the respective sample locations, both of which is unknown. It is evident though, that the whole hanging wall sediment package increases in thickness towards the fault providing a larger rock column susceptible to compaction, which counterbalances the larger amount of compaction of fault-distal uncemented sediments. To which degree is speculative in our view.*
- Cenozoic uplift and doming: What is its amplitude? Did it affect only fault-distal sediments or the whole area including the footwall? **These factors would be necessary to know, but to which we cannot provide an answer.***
- The slope angle of 10-15° for fault-proximal sediments is taken from Henstra et al. (2016), as cited. Of course, this is an overestimate, because (a) the slope angle decreases away from the fault, and (b) does not take into account potential drag of sediments along the fault. A slope angle of 6° would lower the depth of cementation to ~490 m. We chose to perform the calculation with these steep fault-proximal values to provide a number for maximum depth. Therefore, we regard our assumption of calcite cementation in a burial depth <~1000 m as reasonable, but removed "confidently" from the MS.*

4. All in all, the reference in line 285 of confident estimation of burial depth seems a bit of an overstatement. Furthermore, the absence of quartz overgrowths is not a strong argument for an absence of burial; there could have been burial but no quartz-rich fluids. All this leads me to recommend that there has to be a better attempt at constraining the burial history, based on what is known of the structural evolution of the basin and the overlying sediments. This is also important for interpretation of fluid temperature and formation temperature. In a rift basin, geothermal gradients can be 50°C/km, so a clumped isotope temperature of ~55°C could be equivalent to a burial depth of <1 km (ie. the fluid need not necessarily be hydrothermal). The argument for the geothermal gradient in the text is a bit muddled, as it doesn't specifically separate the likely geothermal gradient of the basin from the heat flow along the fault and the resultant temperature of the fluid.

- Quartz overgrowth: Silica for quartz cement is commonly regarded as deriving internally from the sandstone due to dissolution of feldspar and lithic grains, and quartz grain dissolution at quartz/quartz and, more effectively, at quartz/mica contacts (e.g., Walderhaug, 1994; Oelkers et al., 1996; Bjørkum et al., 1998; Harwood*

et al., 2013). As the sandstone itself is able to provide sufficient silica, and quartz cementation is controlled by crystal growth rate and not by production and transport of dissolved silica, the silica supply is not seen as a limiting factor for quartz cementation (e.g., Walderhaug, 1996, 2000; Lander et al., 2008; Taylor et al., 2010; now added to the manuscript). This also agrees with observations that formation waters are typically saturated or oversaturated with silica (e.g., Bazin et al., 1997a, 1997b; Land, 1997; Houston et al., 2007; Palandri and Reed, 2001). Instead, it is shown that the quartz cement crystal growth rate can be well described as a function of time, temperature, and nucleation surface area (e.g., Walderhaug, 1996, 2000; Lander et al., 2008; Ajdukiewicz and Lander, 2010; Harwood et al., 2013), which is successfully applied in diagenetic prediction modelling in industry and research (e.g., Lander et al., 2008; Tobin et al., 2010; Taylor et al., 2015; English et al., 2017; and many more).

Therefore, we disagree with the reviewer and do regard the absence of quartz overgrowth as a valid argument that the analysed sediments have not been exposed to temperatures above 100°C. [lines 359-366]

Further, we note that we do not use the absence of quartz overgrowth as a burial depth measure, which the reviewer's comment implies, but only as a temperature measure.

- b. Geothermal gradient: The reviewer suggests to assess the thermal structure of the basin and burial depth of the sediments with the proposition of a likely geothermal gradient (c.f. reviewer comment to line 302 in manuscript). However, the reviewer notes as well that the geothermal gradient can be highly variable, which is indeed documented elsewhere in rift zones (e.g., Wheildon et al., 1994; Jones, 2020). Hence: what is a "likely" geothermal gradient? We think that any number would be speculative and therefore refrain from such a calculation.

We acknowledge that in this regard our calculation of a geothermal gradient using cement temperature and estimated burial depth might not hold the most added value. We therefore removed this part in the revised MS to keep the focus of this paragraph on the indication that fluid temperature was spatially variable in the hanging wall.

5. A deeper evaluation of the likely fluid source is needed. Using the isotope data, remind the reader of the range of values and differences between the cements and the veins and cite the $\delta^{18}\text{O}_{\text{water}}$ of Cretaceous seawater and assess the likely $\delta^{18}\text{O}_{\text{water}}$ of meteoric water at the paleolatitude the basin was at. Use G-7 as a likely 'pure' meteoric water but justify this on the basis of the palaeolatitude.

We improved these sections and added information on seawater $\delta^{18}\text{O}$ for the Cretaceous and meteoric $\delta^{18}\text{O}$ with respect to paleolatitude. [lines 382-395 and lines 419-524]

6. More use should be made of the trace element data, which I felt was really not integrated into the interpretation as well as it could have been. It is striking that the concentration of Sr is very low (how does this align with cementation from seawater?) whilst Fe concentrations are very high. Why? What does this tell us about the fluids? They must have been reducing, but the source of the Fe should also be discussed.

We expanded chapter 5.3 with a discussion about the source of Fe and Mn and the potential reason for the low Sr concentrations. [lines 497-505]

Incorporation of Sr into calcite is significantly temperature- and precipitation rate-controlled with an uptake decreasing with temperature and increasing with precipitation rate (e.g., Swart, 2015, and references therein; Beck et al., 1992). Hence, the low Sr concentration in the cements and veins may be due to the elevated precipitation temperature, but it is our understanding that it does not allow to decipher the fluid source.

The source of Fe is most likely biotite, which is a common component of the sandstone as seen in the thin sections. This may also explain the large variability of Fe concentration across the samples: depending on the local quantity of biotite and its reaction time with the fluid, Fe may have entered the fluid and subsequently precipitated with calcite to a greater or lesser extent. (see also our response to the next comment).

Pyrite is common along the biotite indicating, that (a) biotite released Fe, and (b) a reducing environment prevailed. A reducing environment also allows for the availability of Fe²⁺ which can subsequently be incorporated into the calcite.

- a. *We added a figure with BSE images of sample G-38 showing the presence of pyrite along biotite, which is abundant in the sample mount. Biotite flakes are expanded with calcite surrounding the lamellae.*

7. I wasn't convinced by the idea of diffusion from cement into veins to give similar trace element concentrations. How would this work? If the cement had precipitated prior to fracturing – as it has to have done to have increased tensile strength – why would trace elements diffuse into the fluids precipitating calcite in the veins? Could it not just be that calcite in the matrix and the fractures was precipitated from similar fluids?

- a. *Since both reviewers raised doubts in this matter, we understand that some more explanations are necessary: [lines 528-545]*

Diffusion of mass from local wall rock into a fracture is seen as a common source of vein material and a series of factors promote such diffusion, e.g. chemical and pressure gradients between wall rock and fluid-filled fracture (e.g., see reviews of Oliver and Bons, 2001, and Bons et al., 2012, and references therein).

Further, calcite is highly susceptible to pressure solution (e.g., Croizé et al., 2015; Toussaint et al., 2018), with the formation of stylolites as its most prominent resultant in carbonate rock. As pressure solution is known to start at shallow burial depth (e.g. Ebner et al., 2009; Croizé et al., 2015), it would be rather surprising if the calcite cement in the sandstone was not subject to a certain degree of pressure solution.

- b. *For the suggestion of similar fluid for cement and veins, we see two problems:*
 - i. *For, e.g., sample G-38 there is an age difference between cement and vein of ~20 Myr. How likely is it that a fluid has a remarkably similar minor element concentration after such a long time period?*
 - ii. *Sample G-36 is taken ~2 m away from G-38, but especially the Fe concentration of the cements and veins varies significantly between G-36 and G-38. Why would a similar fluid result in very local element variations from sample to sample but not show variations from wall rock to vein within one sample (and keeping in mind the large age difference between wall rock and vein)?*
- c. *As stated above in bullet #6, the Fe in the calcite cement has likely derived locally from the alteration of biotite. The Fe concentration would therefore depend on the proximity of the analysed cement to biotite flakes. We revisited the 1-inch mounts of*

G-36 and G-38 used for the U-Pb and minor element analysis and note a very large quantity of biotite in the wall rock of G-38 (see the new figure 5).

d. Therefore, we decide to keep our interpretation, but expand this section with more detailed explanations. [lines 528-545]

8. More consideration needs to be given to the source of the carbonate for calcite precipitation. I agree that an organic source seems likely on the basis of $\delta^{13}\text{C}$ but is this feasible based on what we know of the sediment source and depositional process? What does the isotope data tell us of the burial depth and redox conditions? Is cementation taking place in the zone of bacterial oxidation or sulphate reduction?

We expanded this section of the discussion, noting that organic matter is common in the Lindemans Bugt Formation (ammonites, bivalves, belemnites, transported plants and wood) and that the presence of pyrite indicates organic degradation in the sulphate reduction zone. [lines 493-496]

9. A paragenetic sequence is needed to show the relative timings of the phases (backed up by images to support the interpreted paragenetic sequence), and to clearly illustrate the relative timing of matrix calcite cementation, vein calcite cementation, feldspar overgrowths, compaction, etc. Some more description of the veins is also needed to justify –within the paragenetic sequence – that the cements are passive fill; ie. the text and figures should demonstrate that vein filling calcite has undergone no structural deformation, there are no wall rock inclusions, stretch fibres or cross-cutting relationships suggesting offset, etc.

We expanded the description of the cements and veins, added respective subfigures and a paragenetic sequence. [lines 210-230 and lines 235-243]

Minor points

- Wollaston Forland – Wollaston Foreland?
 - *Wollaston Forland is the Danish name for the region. The word “forland” is a landform, and different to the English word “foreland”.*
- Reference is made in the introduction to hanging wall sediments being porous and permeable whilst the basement is impermeable. I agree that unconsolidated sediments are porous, but are they always permeable? Deep water sediments might have low permeability.
 - *We agree with this statement, but also emphasize that the Lindemans Bugt sediments and fault-proximal syn-rift sediments are no typical deep water sediments. Our statement was more targeting towards the relative permeability difference between crystalline and metamorphic footwall versus unconsolidated sediments, which we believe is fair to say as being high. We altered the sentence to clarify our statement.*
- Methods: how many samples and what was sampling strategy and how many thin sections? Was a separate sub-set of polished sections made up for CL and Raman? i.e. were there 30 sections in all or were 30 polished sections made from a larger sample set of thin sections? How many samples were of vein calcite and how much were of matrix-cemented sandstone or had both matrix cements and veins in the sample?
 - *We expanded this section with more details.*
- Please don't use structural phrases as sedimentological descriptors - ie. 'early syn-rift marine sediments' is meaningless. They are marine sediments deposited during the early syn-rift.

- *We would like to stick to these phrasings. Terms like “syn-rift sediments/deposits/strata” are well established and frequently used in the literature (e.g. Jackson et al., 2002; Karner et al., 1997; Sharp et al. 2000; Ravnås et al, 2000).*
- The width of the cementation zone is estimated to be larger than previously (1.5 km rather than 1 km) in results but without an explanation of why. Please provide the observations to support this statement
 - *This statement is based on the visit of new outcrops with regard to the 2014 field trip of Kristensen et al. (2016). We clarified this in the manuscript.*
- In the results, please describe directions using cardinal directions rather than ‘farther into the basin’ as the latter is interpretive.
 - Corrected.
- I’ve made lots of comments and suggested edits in the annotated manuscript, including some places where interpretation has crept into the results.
 - *Highly appreciated! We followed most of the suggestions. Other comments have been addressed with the responses above.*
 - Line 269: explanation feels unfinished. You mean that there was tensile failure, cementation and as a result re-setting of the cement age? But if so, then why weren't the matrix cement ages of other samples reset?
 - *This is an excellent question, which we unfortunately cannot give an answer to. In the literature known to us and discussions with colleagues, we have the impression that the process of recrystallization is known, yet the driving factors are rather poorly understood.*
 - Line 395: there are a lot of oversized pores in Fig. 4 - are these due to grain dissolution or a function of plucking during thin section preparation?
 - *These pores are indeed the result of grain plucking during thin section preparation. We now clarify this in the figure caption.*
 - Line 398: if so, why did they not precipitate until they entered the LB Formation?
 - *This would be hard to say. Pressure? Temperature? pH?*
 - Fig 11: How viable is this? It looks as though groundwater is flowing directly through the plateau basalt, but is this feasible? What is the permeability of the basalt? How thick was it?
 - *These are reasonable questions to which we cannot really provide an answer to. It may also be that meteoric water was flowing laterally into the basin, e.g. from farther distance through the relay ramp between the Dombjerg and Thomsenland faults. We modified the arrow with a dashed tail and a question mark and added a remark to the figure caption.*
 - Fig. 11: all this looks (in A-C at least) as though there is flow of oxic seawater, but the abundance of Fe suggests reducing conditions. This needs more explanation
 - *The water may be oxic when entering the sediment, but usually becomes anoxic after a few cm to m into marine sediment, which includes coastal and shelf settings (e.g. Tyson, 1995, "Sedimentary Organic Matter"; Libes, 1992, "An Introduction to Marine Biogeochemistry", and we are not aware of a case study showing a redox boundary in deeper burial depth). In the revised MS we have now also clarified that calcite precipitated in a reducing environment.*

REFERENCES

Ajdukiewicz, J. M., & Lander, R. H. (2010). Sandstone reservoir quality prediction: The state of the art. AAPG bulletin, 94(8), 1083-1091.

- Bazin, B., Brosse, É., & Sommer, F. (1997). Chemistry of oil-field brines in relation to diagenesis of reservoirs 1. Use of mineral stability fields to reconstruct in situ water composition. Example of the Mahakam basin. *Marine and Petroleum Geology*, 14(5), 481-495.
- Bazin, B., Brosse, É., & Sommer, F. (1997). Chemistry of oil-field brines in relation to diagenesis of reservoirs—2. Reconstruction of palaeo-water composition for modelling illite diagenesis in the Greater Alwyn area (North Sea). *Marine and Petroleum Geology*, 14(5), 497-511.
- Bjørkum, P. A., Oelkers, E. H., Nadeau, P. H., Walderhaug, O., & Murphy, W. M. (1998). Porosity prediction in quartzose sandstones as a function of time, temperature, depth, stylolite frequency, and hydrocarbon saturation. *AAPG bulletin*, 82(4), 637-648.
- Bons, P. D., Elburg, M. A., & Gomez-Rivas, E. (2012). A review of the formation of tectonic veins and their microstructures. *Journal of Structural Geology*, 43, 33-62.
- Croizé, D., Renard, F., & Gratier, J. P. (2013). Compaction and porosity reduction in carbonates: A review of observations, theory, and experiments. In *Advances in Geophysics* (Vol. 54, pp. 181-238). Elsevier.
- Ebner, M., Koehn, D., Toussaint, R., Renard, F., & Schmittbuhl, J. (2009). Stress sensitivity of stylolite morphology. *Earth and Planetary Science Letters*, 277(3-4), 394-398.
- English, K. L., English, J. M., Bonnell, L. M., Lander, R. H., Hollis, C., Redfern, J., ... & Cherif, R. Y. (2017). Controls on reservoir quality in exhumed basins—an example from the Ordovician sandstone, Illizi Basin, Algeria. *Marine and Petroleum Geology*, 80, 203-227.
- Harwood, J., Aplin, A. C., Fialips, C. I., Iliffe, J. E., Kozdon, R., Ushikubo, T., and Valley, J. W.: Quartz Cementation History of Sandstones Revealed By High-Resolution Sims Oxygen Isotope Analysis, *Journal of Sedimentary Research*, 83, 522-530, doi:10.2110/jsr.2013.29, 2013.
- Houston, S. J., Yardley, B. W., Smalley, P. C., & Collins, I. (2007). Rapid fluid-rock interaction in oilfield reservoirs. *Geology*, 35(12), 1143-1146.
- Jackson, C. A. L., Gawthorpe, R. L., & Sharp, I. R. (2002). Growth and linkage of the East Tanka fault zone, Suez rift: structural style and syn-rift stratigraphic response. *Journal of the Geological Society*, 159(2), 175-187.
- Jones, D. J. R. (2020). A summary of the East Africa Rift Temperature and Heat flow model (EARTH).
- Karner, G. D., Driscoll, N. W., McGinnis, J. P., Brumbaugh, W. D., & Cameron, N. R. (1997). Tectonic significance of syn-rift sediment packages across the Gabon-Cabinda continental margin. *Marine and Petroleum Geology*, 14(7-8), 973-1000.
- Land, L. S. (1997). Mass transfer during burial diagenesis in the Gulf of Mexico sedimentary basin: an overview.
- Lander, R. H., Larese, R. E., & Bonnell, L. M. (2008). Toward more accurate quartz cement models: The importance of euhedral versus noneuhedral growth rates. *AAPG bulletin*, 92(11), 1537-1563.
- Oelkers, E. H., Bjorkum, P. A., & Murphy, W. M. (1996). A petrographic and computational investigation of quartz cementation and porosity reduction in North Sea sandstones. *American Journal of Science*, 296(4), 420-452.
- Oliver, N. H., & Bons, P. D. (2001). Mechanisms of fluid flow and fluid–rock interaction in fossil metamorphic hydrothermal systems inferred from vein–wallrock patterns, geometry and microstructure. *Geofluids*, 1(2), 137-162.

- Palandri, J. L., & Reed, M. H. (2001). Reconstruction of in situ composition of sedimentary formation waters. *Geochimica et Cosmochimica Acta*, 65(11), 1741-1767.
- Prosser, S. (1993). Rift-related linked depositional systems and their seismic expression. *Geological Society, London, Special Publications*, 71(1), 35-66.
- Ravnås, R., Nøttvedt, A., Steel, R. J., & Windelstad, J. (2000). Syn-rift sedimentary architectures in the Northern North Sea. *Geological Society, London, Special Publications*, 167(1), 133-177.
- Sharp, I. R., Gawthorpe, R. L., Underhill, J. R., & Gupta, S. (2000). Fault-propagation folding in extensional settings: Examples of structural style and synrift sedimentary response from the Suez rift, Sinai, Egypt. *Geological Society of America Bulletin*, 112(12), 1877-1899.
- Taylor, T. R., Giles, M. R., Hathon, L. A., Diggs, T. N., Braunsdorf, N. R., Birbiglia, G. V., ... & Espejo, I. S. (2010). Sandstone diagenesis and reservoir quality prediction: Models, myths, and reality. *AAPG bulletin*, 94(8), 1093-1132.
- Taylor, T. R., Kittridge, M. G., Winefield, P., Bryndzia, L. T., & Bonnell, L. M. (2015). Reservoir quality and rock properties modeling—Triassic and Jurassic sandstones, greater Shearwater area, UK Central North Sea. *Marine and Petroleum Geology*, 65, 1-21.
- Tobin, R. C., McClain, T., Lieber, R. B., Ozkan, A., Banfield, L. A., Marchand, A. M., & McRae, L. E. (2010). Reservoir quality modeling of tight-gas sands in Wamsutter field: Integration of diagenesis, petroleum systems, and production data. *AAPG bulletin*, 94(8), 1229-1266.
- Toussaint, R., Aharonov, E., Koehn, D., Gratier, J. P., Ebner, M., Baud, P., ... & Renard, F. (2018). Stylolites: A review. *Journal of Structural Geology*, 114, 163-195.
- Walderhaug, O.: Precipitation rates for quartz cement in sandstones determined by fluid-inclusion microthermometry and temperature-history modeling. *Journal of Sedimentary Research*, 64, 324-333, doi:10.2110/jsr.64.324, 1994.
- Walderhaug, O. (1996). Kinetic modeling of quartz cementation and porosity loss in deeply buried sandstone reservoirs. *AAPG bulletin*, 80(5), 731-745.
- Walderhaug, O. (2000). Modeling quartz cementation and porosity in Middle Jurassic Brent Group sandstones of the Kvitebjørn field, northern North Sea. *AAPG bulletin*, 84(9), 1325-1339.
- Wheildon, J., Morgan, P., Williamson, K. H., Evans, T. R., & Swanberg, C. A. (1994). Heat flow in the Kenya rift zone. *Tectonophysics*, 236(1-4), 131-149.

Author response to comments of Reviewer 2 on “Fault-controlled fluid circulation and diagenesis along basin bounding fault systems in rifts – insights from the East Greenland rift system” by Salomon et al. (response indented and in italic)

1. The description of cements should be highly improved and the use of terminology more accurate. Drusy calcite means pore-filling calcite crystals increasing in size toward the center, what do you mean with coarse calcite? Which is the difference with drusy calcite? Do you mean maybe blocky calcite? In any case, size and morphology of crystals should be given. What about the CL of these calcite cements? What is the colour, is it homogeneous or zoned? Though they have different textures, are they the same cement or are there different cements? Are there differences in the CL for instance from near-fault areas to distal-fault areas? After calcite cements, you talk about feldspar overgrowths, feldspar dissolution, quartz overgrowth and quartz dissolution in both cemented and uncemented areas. The way it is now written this section is confusing. In my opinion, you should establish the paragenetic sequence in cemented and uncemented areas and describe it properly, in order, and with all the information. All this information is very important to validate your data. For instance, the two younger ages obtained in calcite cements, are really a recrystallization process or a later cement filling the remaining porosity?
 - a. *CL color: the color is fairly homogenous across the cement within a sample. We refrain from comparing the CL from sample to sample as we were not able to adjust a stable gun current for all samples. Therefore, we cannot really provide an answer. Yet, given the variability of Fe and Mn concentration across the samples, variations in luminescence should be expected.*
 - b. *Recrystallization: For sample G-9, we believe the cross-cutting relationship provides a strong argument for recrystallization, with a “young” ~104 Ma cement age and an “old” 115 Ma vein generation cutting through the cemented rock. For sample TBK2, such a relationship could not be established, as this sample does not host a vein. Given its similar cement age (~103 Ma) to the G-9 cement, and the equant spar to poikilotopic calcite texture, we argue that recrystallization seems feasible here as well. However, we certainly acknowledge that these latter points are no direct proof of recrystallization and is only our interpretation. We cannot fully exclude the possibility of a second cement growth phase for sample TBK2. We clarify this in the revised manuscript.*
 - c. *Other diagenetic features: We remodeled this section, added more information, and a paragenetic sequence. [lines 210-230]*
2. The same comments can be applied in the following section about veins. You need to characterize the different generations of veins. Can you quantify vein density? Increases towards the main fault? I guess yes. How is the calcite or dolomite filling these veins (size and crystal morphologies, texture, CL)? Veins have one or several cements? Are they petrographically similar or different to host rock cement? What about fracture shapes and lengths? How is the contact between the vein and the host rock? Is it abrupt or gradual? What is the behavior of your veins (opening? Shear?)? How many generations of veins are present? You talk about two

generations near the basement, what about in more distal areas? Looking at figure 5, it seems that you have at least 3 different calcite cements in veins plus a dolomite cement.

- a. Vein density: The vein density has been assessed by Kristensen et al (2016) and we mention it in the geological setting chapter (vein density does indeed increase towards the fault).
- b. Vein descriptions: We expanded this section with more detailed information. [lines 235-243]

3. In this sense of distinguishing calcite cement generations in both host rocks and veins, it is surprising to me that you have not done the basic stable isotope analysis with a $\delta^{18}\text{O}$ - $\delta^{13}\text{C}$ crossplot. If you do this, you have two populations one around -5‰ in $\delta^{18}\text{O}$ and $\delta^{13}\text{C}$ values between -25 and -15‰ (group A) and another around -11‰ in $\delta^{18}\text{O}$ and $\delta^{13}\text{C}$ values between -15 and -10‰ (group B), which in turn are different from the calcite vein of 50 Ma, the vein in the transfer zone and the veins near the fault core. It is true that when you add ages it gets more complicated and in different samples one can see opposite trends from A to B of different ages. But this has to mean something...moments of major inputs of meteoric fluids at different times?

The reviewer points to two populations in the comparison of carbonate $d^{18}\text{O}_{\text{VPDB}}$ vs $d^{13}\text{C}_{\text{VPDB}}$. The clumped isotope results reveal that this is a formation temperature effect and is not indicative for different fluids. For assessing the fluid source (e.g. marine or meteoric), the fluid $d^{18}\text{O}_{\text{VSMOW}}$ data has to be looked at, which is calculated from carbonate $d^{18}\text{O}_{\text{VPDB}}$ using the determined clumped isotope formation temperatures. These populations diminish if the temperature effect is taken into account and a comparison of fluid $d^{18}\text{O}_{\text{VSMOW}}$ and carbonate $d^{13}\text{C}_{\text{VPDB}}$ is made (which needs to be done if the fluid source should be evaluated). A slight trend might be visible in the fluid $d^{18}\text{O}$ vs carb $d^{13}\text{C}$ from very low $d^{13}\text{C}$ and high $d^{18}\text{O}$ to low $d^{13}\text{C}$ and low $d^{18}\text{O}$, which basically reflects the data distribution shown in Fig. 7c,d (now 9d,e) and might be caused by meteoric inflow from the footwall (but as said, the data set is limited and this interpretation should be taken with care).

We now include the fluid $d^{18}\text{O}_{\text{VSMOW}}$ vs carbonate $d^{13}\text{C}_{\text{VPDB}}$ cross plot in figure 7 (now 9), as we agree with the reviewer, that it nicely shows the differences between Eocene vein, fault core veins, basement vein and the rest of the samples. [lines 293-299 and lines 388-395]

Regarding these two sections, figures 3, 4 and 5 are disordered in relation to the text. You call first 3c, then 3e, 4b, 4c, 4d,f , 3b, 5a,b and then 3a! It should be reorganized so figures are called in order.

We reordered the subfigures of figure 3. The main figure order in the text from 3-5 is correct, and in our opinion it is passable that occasionally single subfigures are referred to out of order.

Line 224: you interpret that sample TBK2cem is recrystallized. Recrystallization is an interpretation and should be discussed in the discussion section and not introduced in the results. However, I think

you should describe well these samples (TBK2 and G9cem) to justify that they are not a second cement generation filling the remaining porosity and support recrystallization.

We removed the interpretation from the results chapter and expanded the description of the cements. [lines 210-214]

With regard to elemental composition, you cannot characterize all your veins in the hanging wall together, as you have different cement generations (i.e. G36 and G22 with different CL (fig.5) and different stable isotopy). Moreover, some of them have important CL zonations that are going to imply strong variations at least in Mn and Fe.

As stated above, a comparison of CL color from sample to sample is difficult. Within a vein, there is a certain degree of zonation, which is also reflected in the minor element data (e.g., see the supplementary figures). Growth zonation is mentioned in line 241 and shown in figure 7. Due to the circumstances with the CL analysis stated above, we refrain from further discussing CL color.

In our response to the other review, we outline that the Fe concentration in the calcite cement in the wall rock is likely dependent on the distribution of biotite clasts (see our clarifications to possible diffusion). Since we argue, that the Fe concentration of the vein calcite is reflecting diffusion, the composition of the fluid in the fractures may be variable, depending on the fluids interaction with the local wall rock and the fluid flux. [lines 497-505 and lines 528-545]

I agree with the authors that cementation started soon after the deposition of the sediments, I think that the dates of TBK1cem, G-38cem and G36cem indicate this. Also veining started at the end of the rift climax stage as denoted by G10v1. However, I still have concerns about the recrystallization fact (possibly because of the lack of a good description. I think you should describe better these two samples G-9cem and TBK2cem, also adding good pictures). Is it possible that cementation occurred at different times at different stratigraphic levels in a heterogeneous way? I mean, is it possible that the beds where sample G9cem or TBK2cem are, were cemented after the bed of G38cem for instance? Or that there are two cement generations? Could be this date of 115.5 Ma the wrong one? Or if there is a recrystallization, what is the cause of this patchy, local recrystallization?

Surely, the matter on potential recrystallization is not super clear. Sample TBK2 derives from the same bed as TBK1 and ~1m apart from each other, but this cannot truly hold as evidence for simultaneous cementation, as the bed may have gotten fully cemented in two phases. For sample G-9, the story is more clear: the wall rock is cut by the vein and therefore must have been cemented prior to fracturing. We see no indication that the age of vein G-9v4 might be wrong.

We improved the description of the cements and added two more representative photos of cements of which we obtained ages (G-9 and G-36). When comparing the cement texture of which we obtained ages from, we find it intriguing that the only samples with major equant spar to poikilotopic cement textures are G-9 and TBK2. Hence, we stick to our interpretation of recrystallization, although, as said above, we cannot fully exclude a second growth phase

for TBK2. We rewrote this section in the discussion to clarify and acknowledge this circumstance. [lines 210-216 and lines 335-343]

When using U-Pb dating in fractures and veins, usually we don't know whether we are dating fracturing or fluid flow (I have had the same problem). You discuss this fact in a certain way when you say that maybe you have fracturing during the rift climax and then cementation during the postrift. However, I think that your reasoning is not good enough because you base that veining (fracturing+cementation) occurs during the postrift because you have one vein cemented in the synrift and then more veins should be cemented (it is highly probable that there are more veins during the synrift, it is a sampling bias). I think that the key point is the texture of veins. Veins with crackseal texture are a clear evidence of opening and immediate cementation. You said you have some veins with this texture. Do you have dates of this texture in the postrift? In veins with just an opening mode is more complicated. I think it could be good to add a column in table 1 indicating the vein texture. Anyway, I think that here the key point to highlight with your data is that cementation started soon after deposition followed immediately by veining, which lasted during the postrift.

We fully agree, that in case of a larger sample suit, we would most likely have more veins with a syn-rift age. But probably also more of a post-rift age. We are not so sure, if it is really "highly probable" that with more samples we would see an even age distribution of veins from the syn-rift to the post rift. But sure, we cannot exclude this possibility. We added a sentence to the discussion to clarify this. [lines 407-408]

We do have ages of crack-seal growth phases (8 in total) and called them "reopening vein" in table 1 and figure 6. We refrain from using the term "crack-seal vein" here, to avoid confusion, whether or not this texture includes the first vein generation (i.e. the "initial vein"). Other veins have multiple growth zones (termed "continuous growth vein" in table 1 and fig. 6) and U-Pb ages are consistently in line with the relative growth formation (which also applies to cross-cutting relationships, where visible, in the crack-seal veins). Therefore, we do believe that the determined ages are the formation ages and not indicating later fluid flow.

Line 341: your explanations only work if you maintain the same water composition too. With regard to the source of calcium and CO₂ for calcite precipitation (seawater vs Permian carbonates). Why you haven't done ⁸⁷Sr/⁸⁶Sr isotope analyses? It could be a good way to discern the source and the level of fluid-rock interaction.

The paragraph starting with line 341 concerns the temperature variations across the hangingwall vein samples. The water composition has no effect on the clumped isotope signal, as the D₄₇ ratio is temperature dependent.

We agree that Sr isotopy might provide useful data for such evaluation. However, the low Sr concentration in the calcite deterred us from going at it, as it was a tough challenge collecting sufficient pore-filling calcite material from the sandstone samples. We therefore had to set priorities and decided to use the material for the clumped isotope analysis.

d13C values are really low, up to -23‰, in your host rock cements and veins indicating organic matter oxidation. Where is contained this organic matter? In the own Lindemans Bugt Fm or in units below? Any idea about TOC contents or HC presence in the area?

We added “Organic matter is common in the Lindemans Bugt Formation, composing mostly of ammonites, bivalves, belemnites, and transported plant and wood fragments (Pauly et al., 2013; Henstra et al., 2016) [...]” [lines 493-496]

HC presence is not known and seems unlikely.

The low d13C does not necessarily reflect oxidation of organic matter, but could also be caused by reduction of organic matter. The latter seems more likely due to the high concentration of Fe in the calcite and the presence of pyrite (now described in the revised manuscript).

You base your hypothesis of diffusion on the similarity of the elemental geochemistry between veins and their respective host rocks. I have my doubts about this interpretation, don't you think that an easier explanation is that cement and veins are derived from the same type of fluids? I also think that you can extract more information of these data (i.e. redox conditions, fluid origin...).

Please see our comment in our response to the other review, where we clarify and strengthen the arguments for diffusion.

Figure 11, in my opinion, needs some modifications to be more representative of your story. In A, you establish an in-fault circulation of surficial fluids and upward metamorphic fluids. The latter are sustained by your data and discussed in the text but what are the evidence for the surficial fluids? If any, it should be discussed also in the text. Minor graphical comment: As the picture is in 3D, you should maybe paint these metamorphic fluids along the fault plane (as you have done with your in-fault circulation). In B, the arrow for the upflow of metamorphic fluids should be removed, right? Your data and your discussion points towards the presence of seawater and a mixing of seawater and meteoric fluids that increases towards the fault. This entrance of meteoric fluids through the fault zone that diminishes towards the basin should be illustrated. The same for C. I think there should be another sketch before D to illustrate veining during the postrift with their respective fluid origin to complete your story.

The arrow indicating the flow path of in-fault circulation is maybe misleading, as we did not want to argue for surficial fluids, but rather for in-fault marine fluid circulation. We now clarify this with the description within the figure.

Upflow of metamorphic fluids in figure B: figure B aims at still representing the faults activity (the hangingwall basin is still deepening), and therefore fluid pathways should still have existed for metamorphic fluids.

Graphical modification for metamorphic fluids: We agree, but have to admit that this is where the first authors drawing skills have reached their limit.

Inflow of meteoric fluids: In the discussion, we are careful with the interpretation that the data shows an influx of meteoric groundwater from the footwall into the hanging wall and therefore want to avoid adding this to the sketch.

Fifth figure: We added a fifth subfigure accordingly. At the same time, a post-rift sediment package is now included, which was missing in the previous version.

Minor comments:

Line 85: mafic and ultramafic rocks (in plural)

corrected

Line 87: dolostones and limestones, or just carbonates, as you prefer but not a mixture

We changed it to carbonates.

Line 90: rewrite description of Bernbjerg Fm, I guess it is marine heterolithic mudstonesandstone turbidites.

We changed the description to "heterolithic deposits of marine origin, as well as alternating basinal mudstones and turbidite sandstones"

Figure 2: in the legend it should appear the blue color in the upper left corner of the image as well as the grey color.

We added this to the figure legend.

Line 141: it is strange that you talk about carbonate vein and calcite cement when what you have inside the vein it is also a cement. I think you should say carbonate vein if you wish and then interparticle calcite cement or host rock cement, or something similar to be more accurate.

Vein material is commonly not referred to as cement (although we are aware that some authors do occasionally use this term). We now clarified in the MS that with cement, we only refer to interparticle calcite.

Where did you performed the clumped isotope analysis?

At the Department of Earth Science, University of Bergen. We added this info in the MS.

Line 179: does the cementation zone go farther into the basin in coarse-grained beds as it seems to be represented in this way in your figure 11?

Yes, since in the fault-distal sediments the cementation is confined to conglomerate beds. We added this info to the revised MS.

Line 180: alteration zone → cementation zone, it is better if you use the same concept along the manuscript.

We absolutely agree and corrected it.

Line 183: how is the matrix of these matrix-supported conglomerates? Why are they preferentially cemented?

The matrix is commonly fine to coarse sand. We added this to the text.

Preferential cementation: Unfortunately, we have no answer to this. Maybe more nucleation sites? Higher permeability?

Line 188: biogenic calcite clasts → calcite/calcitic bioclasts. What type of bioclasts? Can you give some examples? Are they fragmented? What happens with bioclasts in uncemented areas?

We changed it to “calcitic bioclasts”. We also added that ammonites, bivalves, and belemnites are common in the Lindemans Bugt Fm.

Line 206: Specify that the vein in the transfer zone is developed in the basement

We specified this.

Line 233: specify that this basement vein is the one developed in the transfer zone.

We specified this.

Value for G9 cem is different in the text and in table 1.

Well spotted! Thanks! We corrected it (the one in the table and figure is the correct age).

Line 355: is it possible that the temperature is correct? Sample G34 is located in the transfer zone between two normal faults. These settings are preferential paths for upward migration of hydrothermal fluids.

Yes, this is certainly possible, but as explained in the text we unfortunately cannot validate it. We rewrote this sentence to clarify that this possibility exists.

Line 364: patters → patterns

Corrected

In section 5.3 and 5.4 add ‰ or ‰ at your values.

We added ‰ to all concerned values.

Line 455: solidified → lithified

Corrected

Table 3: young veins → Hangingwall Eocene veins.

Corrected

Table 3: are you sure that G34 has all the elements below the detection limit? It's surprising, I have never seen that before ... Is it not a technical problem?

G-34 was measured in the same run with the other samples and treated the same way during preparation, so we see no reason to question this data.

Fault-controlled fluid circulation and diagenesis along basin bounding fault systems in rifts – insights from the East Greenland rift system

Eric Salomon^{1,2}, Atle Rotevatn¹, Thomas Berg Kristensen^{1,3}, Sten-Andreas Grundvåg⁴, Gijs Allard Henstra^{1,5}, Anna Nele Meckler¹, Richard Albert^{6,7}, and Axel Gerdes^{6,7}

¹Department of Earth Science, University of Bergen, Bergen, Norway

²now at GeoZentrum Nordbayern, University of Erlangen-Nuremberg, Erlangen, Germany

³now at Equinor, Bergen, Norway

⁴Department of Geosciences, UiT The Arctic University of Norway, Tromsø, Norway

⁵now at AkerBP, Fornebu, Norway

⁶Department of Geosciences, Goethe University Frankfurt, Frankfurt, Germany

⁷Frankfurt Isotope and Element Research Center (FIERC), Goethe University Frankfurt, Germany

Correspondence: Eric Salomon (e.salomon@outlook.de)

Abstract. In marine rift basins, ~~rift-climax~~ deep-water clastics (>200 m) in the hanging wall of rift- or basin-bounding fault systems are commonly juxtaposed against crystalline ~~basement~~ ‘basement’ rocks in the footwall. ~~Displacing~~ A distinct feature of such fault systems is therefore the juxtaposition of relatively highly permeable, unconsolidated sediments against relatively low-permeable ~~rock distinguishes these faults significantly from others displacing hard rock~~ basement rocks. Due to limited surface exposure of such fault zones, studies elucidating their structure and evolution are rare. Consequently, their impact on fluid circulation, and ~~in-fault, near-fault, and hanging wall sediment diagenesis~~ diagenesis within and proximal to the fault zone as well as into the hanging wall strata are also poorly understood. Motivated by this, we here investigate a well-exposed strand of a major basin-bounding fault system in the East Greenland rift system, namely the Dombjerg Fault which bounds the Wolleston Forland Basin, NE Greenland. Here, Upper Jurassic and Lower Cretaceous syn-rift deep-water clastics are juxtaposed against Caledonian metamorphic basement.

Previously, a ~1 km-wide zone of ~~increased~~ pervasive pore-filling calcite cementation of the hanging wall sediments along the Dombjerg fault core was identified (Kristensen et al., 2016). ~~Now~~ In this study, based on U-Pb calcite dating, we ~~are able to~~ show that cementation and formation of this cementation zone started during the rift climax in Berrisian/Valanginian times. Using clumped isotope analysis, we determined ~~a cement formation temperature~~ cement formation temperatures of ~30–70°C. ~~Temperatures likely do not relate to the normal geothermal gradient, but to elevated fluid temperatures of upward directed~~ The spread in the formation temperatures at similar formation age indicate variable heat flow of upward fluid circulation along the fault in the hanging wall sediments, which may root in permeability variations in the sediments.

~~Vein formation within~~ Calcite vein formation, post-dating and affecting the cementation zone, clusters between ~125–100 Ma in the post-rift stage, indicating that fracturing in the hanging wall is not directly related to the main phase of activity of the adjacent Dombjerg Fault. Vein formation temperatures are ~~interpreted to reflect a shallow burial depth of the hanging wall~~

~~deposits and range between with~~ ~30–80°C in a similar range as cement formation temperatures. Further, similar minor element concentrations of veins and adjacent cements argue for diffusional mass transfer into fractures, which in turn infers a subdued fluid circulation and low permeability of the fracture network. These results imply that the cementation zone formed a near-impermeable barrier ~~quickly soon~~ after sediment deposition ~~and maintained this state, and that low effective permeabilities~~
25 were maintained in the cementation zone even after fracture formation, due to poor fracture connectivity. We argue ~~that~~ the existence of such a cementation zone should be considered in any assessments that target basin-bounding fault systems for, e.g., hydrocarbon, groundwater, geothermal energy, and carbon storage exploration. Our study highlights that the understanding of fluid flow properties as well as fault-controlled diagenesis affecting the fault itself and/or adjacent basinal clastics is of great fundamental and economic importance.

30

1 Introduction

During rifting and continental breakup, the rift border fault systems that develop may reach lengths of more than hundred kilometers, and accumulate vertical displacements of several kilometers (e.g., Morley, 1995; Ebinger et al., 1999; Whipp et al., 2014). Such fault systems, often guided by pre-existing basement structure (e.g., Ring, 1994; Corti et al., 2007; Salomon et al.,
35 2015; Phillips et al., 2016; Rotevatn et al., 2018), generally exert strong controls on rift geometry, basin physiography, accommodation, and routing of syn-rift sedimentary systems (e.g., Gawthorpe et al., 1994; Sharp et al., 2000). A main character of these fault zones is ~~their significant displacement~~ the juxtaposition of clastic syn-rift sediments against crystalline basement rock (e.g., Gawthorpe and Leeder, 2000).

~~Lithology plays an important part in the evolution of fault systems, especially in concert with fluid flow (Indrevær et al., 2014)~~
40 ~~The interaction between lithology, deformation, and fluid flow has attracted numerous studies since the proposition of the seismic pumping mechanism where seismic faulting triggers hydrothermal fluid injection through the fault core (Sibson et al., 1975)~~
~~Research covers fault zones hosted by igneous (e.g., Mitchell and Faulkner, 2012), metamorphic (e.g., Wibberley and Shimamoto, 2003)~~
~~carbonate (e.g., Smeraglia et al., 2016), mature sedimentary rocks or uncemented sediments~~ The influence of rift border faults on fluid flow and wall rock diagenesis has only to a limited degree been studied (e.g., Pei et al., 2015, and references therein;
45 ~~Williams et al., 2015; Hollis et al., 2017~~). It has been shown that faults may serve as significant conduits (Hollis et al., 2017) or as baffles to fluid circulation (Rawling et al., 2001; Pei et al., 2015). Further, faults may comprise an initial high permeability due to intense fracturing and later become impermeable in consequence of veining (Cox, 1995). At the same time, the fault core may experience a different or even a contrasting permeability evolution than the damage zone surrounding the fault core (Sheldon and Micklethwaite, 2007; Indrevær et al., 2014). ~~Studies on syn-rift border faults displacing crystalline and/or~~
50 ~~metamorphic rocks against elastic sediments have contributed to a lesser degree to the understanding of the interaction of faults and fluids,~~ Hollinsworth et al., 2019, and Kristensen et al., 2016, being notable exceptions), which may primarily root in the limited exposure of such fault zones (e.g., Hollinsworth et al., 2019, and Kristensen et al., 2016, being notable exceptions). In such settings, there is a significant permeability contrast from footwall to hanging wall: the crystalline- / metamorphic footwall

is commonly relatively low-permeable or even near-impermeable, while ~~the unconsolidated-~~, in contrast, the unconsolidated
55 clastic sediments in the hanging wall ~~are highly~~ may be relatively more porous and permeable. Therefore, whereas fluid circulation mainly occurs in fractures in the crystalline “basement” footwall, large fluid volumes ~~can~~ may potentially circulate through the pore space in the clastic hanging wall strata.

At the Dombjerg Fault in NE Greenland (Fig. 1), Kristensen et al. (2016) showed that a ~1 km-wide envelope of calcite cement (~~termed “chemical alteration zone”~~) formed in the hanging wall along the fault, which strongly argues for a significant
60 influence of the fault on ~~diagenesis of the adjacent sediments~~ the diagenetic imprint affecting the hanging wall clastics in the proximity of the fault. This is an important observation, as the calcite cementation transforms the sediments from an unconsolidated to a consolidated state. This in turn changes the mechanical properties of the hanging wall rock, and affects how later deformation is accommodated: while deformation bands ~~would form~~ formed in the damage zone within porous, non-cemented clastics, ~~fractures form in discrete fractures formed in the~~ low- to non-porous cemented clastics (Kristensen et al., 2016). It
65 also significantly affects the permeability of the hanging wall ~~elasties~~ sediments: where porous and non-cemented, fluids ~~flow~~ may flow relatively freely through open pore space ~~and-~~ with flow being hampered only by deformation bands; however, where the clastics have low- to no porosity due to cementation, fluid flow becomes increasingly dependent on open fractures in an otherwise impermeable cemented sedimentary rock.

Hence, the identification of such a zone of enhanced cementation has important implications for the evaluation of near-fault diagenesis ~~and for the-~~ fluid flow properties, and for understanding of the linked deformational, diagenetic and fluid flow history of
70 a fault zone. The fact that near-fault diagenesis ~~significantly~~ substantially impacts flow properties ~~;~~ makes it economically significant ~~;~~ and highly relevant in, e.g., the exploration and exploitation of groundwater, hydrocarbon and geothermal resources, and for subsurface carbon storage sites. However, at present, fault seal analyses ~~in reservoirs mostly rely on juxtaposition seals used in, e.g., the oil and gas industry rely mostly on the analysis of the probability for juxtaposition seal~~ and shale smear,
75 neglecting the effect of ~~a cementation zone~~ diagenetic sealing mechanisms (e.g., Sperrevik et al., 2002; Yielding et al., 2010; Karolytė et al., 2020).

In this contribution, we aim to further elucidate the formation of cementation zones along syn-rift border faults. To do this, and building on Kristensen et al. (2016), we here investigate the evolution of the well-exposed cementation zone of the Dombjerg Fault in the Wollaston Forland of NE Greenland, where we combine the analysis of (i) field and microstructural observations,
80 (ii) cement and vein formation temperatures based on clumped isotope analysis, (iii) cement and vein formation ages based on U-Pb calcite dating, as well as (iv) minor element compositions of cements and veins based on electron microprobe analysis. We demonstrate that the cemented envelope formed soon after the deposition of rift-climax sediments at shallow burial depths, with vein formation occurring predominantly in the post-rift stage. We also show that even after fracturing, the cemented envelope ~~formed an effective seal~~ retained low effective permeabilities due to poor fracture connectivity, thus forming a long-lived
85 barrier for fluid flow. The results offer a unique insight into near-fault diagenesis associated with major basin-bounding fault systems in rifts, showcasing the interplay of ~~tectonic and diagenetic processes.~~ deformation, fluid flow and diagenesis.

2 Geological Setting

The study area is located in the Wollaston Forland in NE Greenland and forms part of the East Greenland Rift System (Fig. 1).

90 This rift system has experienced a long-lived extensional history since the late Paleozoic that eventually resulted in the opening of the North Atlantic in the Paleocene–Eocene (e.g., Larsen and Watt, 1985; Surlyk, 1990; Stemmerik et al., 1991) followed by regional uplift of up to several kilometers in Cenozoic times (Christiansen et al., 1992; Thomson et al., 1999). Onshore, the East Greenland Rift System is exposed along ~600 km where a major right-stepping rift-bounding fault system displaces Permian to Cretaceous syn-rift sedimentary rocks against Caledonian metamorphic and crystalline basement (Fig. 1a). In the
95 Wollaston Forland, this rift-border fault system is marked by the ~25 km long Dombjerg Fault with an approximately 3 km vertical throw (Fig. 1b,c; Surlyk and Korstgård, 2013). Activity of the Dombjerg Fault presumably started in the Mississippian and the fault was repeatedly active prior to the onset of the main rift phase in the Middle Jurassic (Rotevatn et al., 2018). To the North, the fault connects with the Thomsenland Fault through a ~10 km-wide transfer zone.

The footwall block west of the Dombjerg Fault (referred to as the Clavering Block; Fig. 1c) comprises Caledonian migmatite
100 gneisses, pegmatites, amphibolites, felsic gneisses, mafic and ultramafic ~~roek-rocks~~ (Surlyk, 1978; Kristensen et al., 2016). East of the fault in the Wollaston Forland, the earliest sediments deposited, though not directly exposed along the fault, are of Permian age and constitute ~~dolomites, carbonates, and anhydrites~~ carbonates and evaporites (Fig. 1b; Surlyk et al., 1986; Surlyk and Korstgård, 2013). These deposits are overlain by a succession of Upper Jurassic to Early Cretaceous rift-related sediments, which is subdivided into (i) early syn-rift~~marine sediments of the-~~, (ii) rift climax, and (iii) late syn-rift deposits
105 (sensu Surlyk and Korstgård, 2013; early syn-rift broadly corresponds with the term 'rift initiation' sensu Prosser, 1993). Early syn-rift marine sediments are of Middle to Upper Jurassic age (Fig. 1b) and constitute mainly shallow marine sandstone (Pelion Formation), alternating thin mudstone and marine sandstone (Jakobsstigen Formation), and ~~marine heterolith and mudstone with sandstone turbidites~~ heterolithic deposits of marine origin, as well as alternating basinal mudstones and turbidite sandstones (Bernbjerg Formation; Surlyk and Korstgård, 2013).

110 Exposed sedimentary rocks in the hanging wall (referred to as the Kuppel-Kuhn Block, ~~Fig; fig.~~ 1c) of the Dombjerg Fault are of Late Jurassic to Early Cretaceous age (Tithonian – Hauterivian), and are mostly sandstones and conglomerates that stratigraphically belong to the up to 3 km-thick Wollaston Forland Group (e.g., Surlyk, 1984). The sediments were derived from footwall erosion and were deposited by gravity flows in a fully submarine environment during the rift climax and late syn-rift phases (e.g., Surlyk, 1978, 1984; Henstra et al., 2016). The Wollaston Forland Group is divided into the rift climax succession
115 of the Lindemans Bugt Formation (mid Volgian–late Ryazanian, i.e. ~148–147 Ma) and the late syn-rift succession assigned to the Palnatokes Bjerg Formation (latest Ryazanian–early Hauterivian; Surlyk, 1984; Surlyk and Korstgård, 2013; Henstra et al., 2016). This study only pertains to the rift-climax deposits of the Lindemans Bugt Formation.

The Lindemans Bugt Formation consists mainly of conglomerates and sandstones that form a clastic wedge bounded to the west by the Dombjerg Fault, extending 10–15 km eastward into the basin before it gradually thins across the tilted crest of the
120 hanging wall block (Fig. 1c). Close to the basin-bounding border fault, the hanging wall clastic succession is ~2 km thick with strata dipping at 10–15° towards the basin axis to the east (Surlyk and Korstgård, 2013; Henstra et al., 2016). Further basin-

ward, the thickness of the succession decreases and the inclination ~~eases~~ decreases with strata being ~~more~~ sub-horizontal. On the adjacent dip-slope of the hanging wall block, the strata display gently dips up to 6° towards the basin axis to the west (Surlyk and Korstgård, 2013; Henstra et al., 2016). Collectively, the thickness and dip variations reflect the asymmetric geometry of the basin, which is typical of basins developing from fault block rotation (e.g., Gawthorpe and Leeder, 2000). Thus, it is reasonable to assume that the basin was deepest close to the border fault, offering available accommodation for a thick succession of gravity flow deposits to accumulate (Surlyk, 1984; Henstra et al., 2016).

Within a ~2 km-wide zone along the fault, the Lindemans Bugt Formation hosts brecciated clasts up to several meters wide, ~~brecciated elasts~~ consisting of metamorphic and crystalline basement rocks, and unsorted boulder to gravel-size conglomerate beds with average thicknesses exceeding 3 m. Some of the thicker conglomerate beds extend far into the basin (Henstra et al., 2016). Further basin-ward, amalgamated conglomerate–sandstone packages give way to normally graded, gravelly sandstone and sandstone beds with tabular geometries (Henstra et al., 2016). Normally-graded, fine-grained sandstone beds alternating alternate with thin mudstone beds to form heterolithic sheet-like units (Henstra et al., 2016) ~~;~~ and typically occur in fault-distal locations, but locally also occur intercalated with the coarse clastics in close proximity to the fault.

The Dombjerg Fault dips ~65° to the ENE (Kristensen et al., 2016) and has an estimated maximum throw of ~3 km to the base of the rift (Surlyk and Korstgård, 2013). Within a zone of ~200 m width, located in basement rock, the fault consists of multiple fault core strands comprising fault gouge and intense brecciation (Kristensen et al., 2016). The footwall damage zone is ~600 m wide comprising veins, fractures, and minor faults at increasing quantity density towards the fault (i.e. from 4 joints and 1 vein per meter outside the damage zone to >50 joints and 20–30 veins per meter near the fault core; Kristensen et al., 2016). In the hanging wall, the sedimentary rock of the Lindemans Bugt Formation is characterized by intense pervasive calcite cementation extending approximately 1 km into the basin. Calcite veins cut through the cemented rock and are overprinted by joints. Their quantity increases from zero joints and veins per meter outside the damage zone to 7 joints and veins per meter near the fault zone (Kristensen et al., 2016).

145 3 Methodology

This study is based on field analyses and samples taken during a 10-day field season in August 2018, supplemented with by samples collected in an earlier field season in 2014. Outcrops were chosen by accessibility and were mostly confined to the hanging wall of the Dombjerg Fault as snow fields covered the footwall. ~~Thin sections of samples~~ In total, 35 polished thin sections were prepared of which 21 comprise only Lindemans Bugt Formation sediments (9 of these are from carbonate-uncemented sediments), 9 comprise both cemented sediment and vein material, and 5 only vein material (3 with hanging wall veins, 1 from fault rock veins, 1 from vein in basement located in the transfer zone; Fig. 2). The thin sections were analyzed through optical microscopy, scanning electron and SEM cathodoluminescence microscopy on a Zeiss Supra 55VP, cold-cathode cathodoluminescence on a Technosyn 8200 Mk II, and Raman spectroscopy on a Horiba LabRAM HR. ~~30 thin sections of samples from the Lindemans Bugt Formation have been analyzed regarding their diagenetic character. 18 of these samples derive~~

155 ~~from the cementation zone, 3 samples from the carbonate-cemented lenses outside the cementation zone, and 9 samples from~~
~~(carbonate-) uncemented sandstone (Fig. 2).~~

U-Pb analysis for calcite dating was performed at FIERCE (Frankfurt Isotope & Element Research Center), Goethe-University
Frankfurt, with a RESOLution 193 nm ArF excimer laser (CompexPro 102) equipped with a two-volume ablation cell (Lau-
160 rrin Technic S155) coupled to a sector field ICP-MS (ElementXr, ThermoScientific). Before the analysis, the samples were
screened, to find suitable areas for further analysis. This was successful on five calcite cement samples and 12 calcite vein
samples, with a total of 25 vein growth phases, of the Lindemans Bugt Formation (we note that we use the term “cement”
exclusively for pore-filling calcite and not for vein calcite throughout this paper). Calcite vein samples of the basement and
near the fault core did not provide appropriate U and Pb signals. Full details of the U-Pb analysis are described in the suppl-
165 ements. All uncertainties are reported at the 2σ level.

Clumped isotope analysis was conducted on 11 carbonate vein (10 calcite, 1 dolomite) and five calcite cement samples. In
two calcite veins, two growth generations were analyzed (samples G-10 and G-36). Of the 11 vein samples, eight derive from
the hanging wall sedimentary rock of the Lindemans Bugt Formation, two from brecciated basement rock close to the fault
core, and one from basement rock in the transfer zone between the Dombjerg and Thomsenland Fault (Fig. 2). Hanging wall
vein samples were chosen to spatially cover the cementation zone as best as possible. The selection of cement samples was
170 guided by the feasibility of mechanically separating sufficient cement from the rock, which was successful on five samples.
Four of these cement samples are from within the cementation zone and one (H-5) from an isolated cemented layer outside the
~~chemical-alteration~~ cementation zone.

Clumped isotope analysis was performed at the Department of Earth Science, University of Bergen, on a Thermo Fisher Sci-
entific MAT-253 Plus isotope ratio mass spectrometer coupled to a Thermo Fisher Scientific Kiel IV carbonate preparation
175 device, where samples are reacted individually with phosphoric acid at 70°C. For each sample, 13–14 replicate measurements
were performed, spread over 6 months. Results were pressure-baseline corrected (Bernasconi et al., 2013; Meckler et al., 2014)
and transferred into the absolute reference frame (Dennis et al., 2011) using carbonate standards (ETH 1-3) measured along-
side the samples, employing their accepted values determined by Bernasconi et al. (2018). All data processing was performed
with the Easotope software (John and Bowen, 2016). For further details of the method, see Piasecki et al. (2019) or Meinicke
180 et al. (2020). The clumped isotope analysis also yields oxygen and carbon isotope values for each replicate, which have been
corrected for drift using the same carbonate standards, with a two-point scale correction ("stretching") applied to $\delta^{18}\text{O}$ results.
Clumped isotope results (Δ_{47}) were averaged by sample and formation temperatures were calculated after Kele et al. (2015),
using the updated version from Bernasconi et al. (2018), for calcite samples and after Müller et al. (2019) for dolomite samples.
For the calculation, we neglected replicates whose Δ_{47} value deviated from the sample average by 3x the standard deviation
185 of the standards, which in total affected only one replicate. As clumped isotope temperatures are determined independently
of fluid isotopic composition, the results can be used in combination with the measured oxygen isotopic values (carbonate
 $\delta^{18}\text{O}_{\text{VPDB}}$) to calculate fluid $\delta^{18}\text{O}_{\text{VSMOW}}$. For calcite samples, fluid $\delta^{18}\text{O}_{\text{VSMOW}}$ was calculated after Kim and O'Neil (1997,
updated with fractionation factor of 1.01025), and for dolomite samples the calibration of Horita (2014) was used. All un-
certainties are presented at the 95 % confidence interval. The uncertainty for fluid $\delta^{18}\text{O}_{\text{VSMOW}}$ is given from the uncertainty

190 propagation using the 95 % confidence intervals of the clumped isotope temperature and carbonate $\delta^{18}\text{O}_{\text{VSMOW}}$ and calculated as

$$\sqrt{\left(\frac{\partial \text{fluid}^{18}\text{O}}{\partial T} \cdot \Delta T\right)^2 + \left(\frac{\partial \text{carb}^{18}\text{O}}{\partial \text{carb}^{18}\text{O}} \cdot \Delta \text{carb}^{18}\text{O}\right)^2} \quad (1)$$

Electron microprobe analysis for minor element concentrations (Mg, Fe, Mn, Sr) of calcite veins and cements was conducted on a Cameca SX100 at accelerating voltage 15kV, beam current 10nA, counting time on peak 20s, and total counting time on
195 background 20s. Detection limits were 300 ppm (Mg), 540 ppm (Fe), 630 ppm (Mn), and 420 ppm (Sr). For each analyzed vein generation 10 points were measured, and 20 points for cements as the latter has shown a larger variability in element concentrations.

4 Results

200 4.1 Cementation zone and diagenetic character of hanging wall sediments

The cementation zone forms an envelope of variable width along the Dombjerg Fault and, based on investigation of additional outcrops in the 2018 field season, we estimate its maximum width to be ~ 1.5 km (Fig. 2), which is ~~a-bit~~ larger than previously ~~assessed (~ 1 km; estimated by~~ Kristensen et al. ~~(2016; i.e. ~ 1 km)~~. Within this zone, calcite cementation is prominently distributed and occurs in sedimentary layers of all grain sizes, while uncemented layers occur occasionally and are usually
205 less than 50 cm thick. At the fault-distal limit of the ~~alteration zone, cementation zone, cementation is mainly confined to conglomerate beds and~~ outcrops show cemented layers with “holes” formerly filled with now-eroded uncemented material (Fig. ~~3e3a~~). It appears that the cemented layers enclosed pockets of calcite-cement free sediments. Farther ~~into the basin to the east~~, calcite cement is absent in the vast majority of outcropping sediments (Fig. ~~3e3c~~) and only occurs occasionally as single isolated lenses in predominantly fine to coarse sand matrix-supported conglomerates.

210 Calcite cement occurs as ~~drusy spar (Fig. 4b) and in a coarse spar to poikilotopic texture (Fig. 4c). Drusy spar micrometer-sized spar, anhedral equant spar with crystal sizes up to 200 μm and as subhedral poikilotopic calcite with crystal sizes up to 800 μm (Figs. 4c-f). Microspar is present in 11-12 of 21 samples, all of which also comprise a varying amount of coarse equant calcite spar. The latter is dominant in four samples.~~ Poikilotopic texture occurs in only two samples from within the cementation zone (samples G-9, TKB2) and in three samples from cemented lenses outside the cementation zone (sample H-5). Notably,
215 sample TBK2 hosting poikilotopic calcite derives from the same outerop bed as sample TBK1 hosting ~~drusy spar (Figs. 2, 4b,c). Biogenic calcite elasts are occasionally present in dominantly microspar (samples taken 1 m apart from each other; figs. 4c,d).~~ Other notable diagenetic features are:

- Feldspar grain dissolution appears in varying degrees and is generally more dominant in the cemented samples and show no signs of dissolution or recrystallization. Feldspar overgrowth, where it is partially replaced by calcite cement. Feldspar overgrowth predates calcite cementation and occurs in both cemented and uncemented samples (Figs. ~~4d,f~~).

220

~~but is commonly more pronounced in the latter sample suit. Feldspar grain dissolution is absent or only occurs to a minor degree in uncemented samples. The calcite-cemented samples comprise minor to major feldspar dissolution (Figs. 4b,c), although complete grain dissolution does not occur. Quartz overgrowth has not been detected (4b,h).~~

- Quartz overgrowth is absent in all samples.

225 • Pyrite is common along biotite grains, which itself is a major constituent of the sandstone (Fig. 5). Calcite cement pervasively fills space between separated biotite lamellae.

- Calcitic bioclasts, that are occasionally present in the samples. ~~Quartz grain dissolution is only a minor component in cemented samples and absent in uncemented samples (Fig. 4).~~, are partially fragmented and show no signs of dissolution or recrystallization.

230 A summary of relative timing of the main diagenetic features is given in figure 6.

4.2 Vein structure and composition

In all outcrops within the cementation zone, calcite veins were found (Fig. ~~3b3d~~), which have an overall NNE to NE trend (67 veins measured in total; ~~Fig~~fig. 2). Outcrop surfaces were exposed in 3-D and we hence conclude that this dominant vein trend is true and not biased by outcrop orientation. Veins exclusively occur in cemented parts of the ~~hosting sandstone and single sandstone~~ and are approximately equally distributed in outcrops with spacing varying in the decimeter to meter scale and do not form clusters. Single vein thicknesses span from <1–70 mm and veins appear as mode I fractures, i.e. possible shear displacement is only observed in 3 of 14 samples. In all cases, the veins have a sharp contact with the wall rock, i.e. wall rock grains are cut by the fracture (Fig. 7). All analyzed veins exhibit at least one generation of elongate to blocky syntaxial crystal growth. Two thirds of the analyzed veins comprise two or more vein growth generations, indicated by either crack-seal texture (i.e. precipitation after reopening of fracture) or growth zonation, as visible in thin section view (Figs. 5a7a,b). Calcite twin density is generally low and slip zones within veins are found in three samples.

235

240

Near the fault core within brecciated basement rock, two vein generations were identified: a syntaxial dolomite vein network that is cross-cut by a younger syntaxial calcite vein network (Fig. 3a). The dolomite network ~~is prominently visible and~~ composes of continuous, anastomosing veins of varying thicknesses up to 30 mm wide (Figs. ~~3a, 5e3e, 7e~~). The younger calcite vein network consists of planar veins with thicknesses of ~1–5 mm (Fig. ~~3a~~) and ~~fills voids within the dolomite veins as well~~ 3e and also envelopes dolomite in the center of dolomite-filled fractures (Fig. ~~5f. As far as visible, the 7f~~). The dolomite veins are not displaced/offset by the calcite veins and the latter are ~~as well~~ not displaced by any other fracture set. In the transfer zone, connecting the Dombjerg and Thomsenland faults (Fig. 2), only one calcite vein was found in a shear fracture that reactivated

250 an older epidote vein situated in basement rock.

4.3 Ages of calcite cements and veins

We determined formation ages of five cement samples and 12 vein samples within the sediments of the Lindemans Bugt Formation (Table 1, fig. 68). As some veins comprise more than one growth generation, as evident by zoning or fracture re-opening (see section 4.2), we obtained a total of 25 growth ages of the 12 vein samples. Age determination of veins within the basement and fault core were not successful due to unsuitable U and Pb signals.

Three cement ages fall within the previously reported depositional age of the Lindemans Bugt Formation (mid Volgian – late Ryazanian; Surlyk, 2003) or close to its depositional age boundary with the Palnatokes Bjerg Formation (late Ryazanian – Hauterivian) with 150.6 ± 9.3 Ma (G-36cem), 143.7 ± 6.5 Ma (TBK1cem), and 139.4 ± 4.9 Ma (G-38cem). The, while two other cement ages are significantly younger with 103.3 ± 2.6 Ma (TBK2cem) and 102.9 – 104.1 ± 3.7 – 1.7 Ma (G-9cem) and most likely reflect calcite recrystallization ages (see discussion chapter 5.1). Of the vein samples, only one falls within the inferred rift stage with 139.3 ± 3.4 Ma (G-10 v1), while the majority of vein ages (both initial formation ages and vein reopening ages) fall within a range of ~ 125 – 90 Ma (Fig. 68). Two vein ages are significantly younger with 50.1 ± 2.1 Ma (G-7) and 49.4 ± 2.1 Ma (G-2), closely post-dating early Eocene plateau basalt extrusion and the onset of continental breakup (Fig. 68).

4.4 Clumped isotope temperatures of calcite cements and veins

Clumped isotope temperatures of five pore-filling calcite cement samples were obtained. Temperatures from TBK1cem and the recrystallized-TBK2cem, which derive from the same outcrop, are $42.0 \pm 10.2^\circ\text{C}$ and $59.0 \pm 9.1^\circ\text{C}$, respectively. G-25cem, sampled at a similar distance to the main fault core, has a clumped isotope temperature of $42.4 \pm 8.8^\circ\text{C}$, G-36cem at the distal margin of the cementation zone has $56.6 \pm 10.9^\circ\text{C}$, and H-5cem, located well into the basin, has $44.5 \pm 9.0^\circ\text{C}$ (Table 2, Fig. 2).

Clumped isotope temperatures of hanging wall veins fall into the range of $36.3 \pm 9.4^\circ\text{C}$ (G-36 v1) and $77.6 \pm 10.1^\circ\text{C}$ (G-22). In the two samples of which two vein generations were analyzed, a temperature increase exists from old to young vein phase (i.e. G-36 from $36.3 \pm 9.4^\circ\text{C}$ to $58.2 \pm 14.1^\circ\text{C}$ and G-10 from $40.3 \pm 7.1^\circ\text{C}$ to $61.5 \pm 10.5^\circ\text{C}$; Table 2, fig. 5a7a). However, taking all samples, including cement samples, into consideration, no clear trend in temperature evolution with time relationship between calcite generation and temperature is visible (Fig. 7a9a), which is also true for the relationship of temperature and distance to the fault core (Fig. 7b9b). The clumped isotope temperature of the basement vein sample G-34, located in the transfer zone, yields $128.7 \pm 19.1^\circ\text{C}$. Near the fault core in the brecciated basement, the clumped isotope temperature of the younger calcite vein (TBK9cal) that cross-cuts the dolomite vein network falls with $68.8 \pm 10.9^\circ\text{C}$ into the range of hanging wall vein temperatures. The older dolomite vein sample TBK9dol diverges from this pattern with a higher temperature of $106.5 \pm 11.9^\circ\text{C}$ (Fig. 5f; 7f; table 2).

4.5 Oxygen and carbon stable isotope values

285 Carbonate $\delta^{18}\text{O}_{\text{VPDB}}$ values range from $-11.3 \pm 0.09 \text{‰}$ to $-6.1 \pm 0.05 \text{‰}$ for cements and from $-12.8 \pm 0.05 \text{‰}$ to $-4.1 \pm 0.09 \text{‰}$ for most hanging wall veins, with the exception of vein sample G-7 with $-21.4 \pm 0.12 \text{‰}$ (Table 2). The basement vein sample G-34 comprises $-18.0 \pm 0.04 \text{‰}$ and the two fault core vein samples have values of $-15.3 \pm 0.33 \text{‰}$ (TBK9dol) and $-11.7 \pm 0.05 \text{‰}$ (TBK9cal).

290 The calculated fluid $\delta^{18}\text{O}_{\text{VSMOW}}$ values range from $-4.3 \pm 1.9 \text{‰}$ to $-0.2 \pm 1.6 \text{‰}$ for cements and $-3.0 \pm 1.7 \text{‰}$ to $+1.9 \pm 2.3 \text{‰}$ for hanging wall veins, while sample G-7 deviates significantly from this suite with $-13.7 \pm 1.5 \text{‰}$ (Fig. 9c; Table 2). The basement sample G-34 as well as the vein calcite sample TBK9cal also fall into this range with $-0.4 \pm 2.1 \text{‰}$ and $-1.8 \pm 1.7 \text{‰}$, respectively. The older vein dolomite sample TBK9dol from the fault core appears to have precipitated from an enriched fluid of $+16.2 \pm 1.6 \text{‰}$.

295 Carbonate $\delta^{13}\text{C}_{\text{VPDB}}$ values range from $-18.2 \pm 0.3 \text{‰}$ to $-9.7 \pm 0.8 \text{‰}$ for cements and $-23.5 \pm 0.5 \text{‰}$ to $-11.3 \pm 0.1 \text{‰}$ for hanging wall veins (Fig. 9c; Table 2). The basement and fault core samples differ significantly from these values with $-5.5 \pm 0.1 \text{‰}$ (G-34), $-4.2 \pm 0.1 \text{‰}$ (TBK9cal), and $-2.2 \pm 0.2 \text{‰}$ (TBK9dol). In general, and bearing in mind the limited data base, samples in the hanging wall might show a slight trend from low carbonate $\delta^{13}\text{C}_{\text{VPDB}}$ and high fluid $\delta^{18}\text{O}_{\text{VSMOW}}$ values to higher carbonate $\delta^{13}\text{C}_{\text{VPDB}}$ and lower fluid $\delta^{18}\text{O}_{\text{VSMOW}}$ values (Fig. 9c). Also, a slight increase in fluid $\delta^{18}\text{O}_{\text{VSMOW}}$ and decrease in carbonate $\delta^{13}\text{C}_{\text{VPDB}}$ with increasing distance to the fault might exist (Figs. 9d,e).

300 4.6 Minor element concentrations of cements and veins

For the minor element concentration analysis, we studied 10 calcite cement samples, 12 hanging wall calcite vein samples, two samples of veins from the fault core (one dolomite, one calcite vein), and one basement calcite vein sample (Table 3, Fig. 810). As some hanging wall samples comprised multiple vein **growth** generations, we measured in total 22 growth generations in the 12 hanging wall samples.

305 Common to all samples is a Sr concentration below or close to the detection limit and will therefore be neglected in the following. Cements comprise element concentration averages of 2429–11862 ppm (Fe), 2866–5045 ppm (Mn), and 1152–7557 ppm (Mg) (Table 3). Hanging wall veins yield similar averages with values of 1436–13598 ppm (Fe), 2515–6719 ppm (Mn), and 401–5180 ppm (Mg). The two Eocene-aged hanging wall veins G-2 and G-7 differ significant with Fe and Mg concentrations being below the detection limit, and Mn concentration below detection in sample G-2, and 2390 ppm in sample G-7. The same
310 accounts for the basement sample G-34 with Fe, Mn, and Mg concentrations being below the detection limit. The fault core vein TBK9cal yields concentrations of 8342 ppm (Fe), 1435 ppm (Mn), and 887 ppm (Mg). Naturally, the older fault core dolomite vein TBK9dol diverges from the other samples with a high Mg and Fe concentration of 112599 ppm and 24556 ppm, respectively, and a low Mn concentration of 1219 ppm.

The comparison of veins and respective cements from the immediate wall rock within a sample shows similar Mg- and Mn-
315 concentrations for a majority of samples (i.e. samples G-4, G-9, G-22, G-25, and G-38; Fig. 89), which also partly accounts for Fe (G-4, G-25, G-38; Fig. 810). Overall, the Fe/Mn/Mg ratio is similar from cement to vein within half of the samples, whereas concentration and ratios differ from sample to sample (e.g., compare G-25 and G-38; Fig. 810). Vein generations

within a sample do not show significant variations in minor element concentrations (supplementary figure S2). No trends in concentration or ratio versus time or spatial distribution are evident.

320

5 Discussion

5.1 Timing and formation environment of the cementation zone

Based on the ~~U/Pb~~ U-Pb calcite cement ages of 150.6 ± 9.3 Ma, 143.7 ± 6.5 Ma, and 139.4 ± 4.9 Ma (samples G-36, TBK1, G-38), the formation of the cementation zone in the hanging wall has likely occurred during or immediately after the deposition of the ~~hosting~~ host sediments of the Lindemans Bugt Formation during the rift climax (~~Fig. 6~~ mid Volgian-late Ryazanian; Surlyk, 2003; Fig. 8). The 150.6 Ma age of G-36 is unrealistic as it predates the Lindemans Bugt Formation, however its error margin reaches well into the time interval over which this formation was deposited (~~Fig. 6; e.g., Surlyk, 2003~~). ~~(Fig. 8; e.g., Surlyk, 2003). The upper formation age of the cementation zone is bounded by the age of vein G-10 v1 with 139.3 ± 3.4 Ma (i.e. close to the upper age boundary of the Lindemans Bugt Formation), as the rock had to be cemented to provide~~ the tensile strength for the discrete fracture to form.

330

The two younger cement ages of 104.1 ± 1.7 Ma (G-9cem) and 103.3 ± 2.6 Ma (TBK2) do not reflect a second cement growth phase, but are interpreted to be recrystallization ages, for the following reasons: In sample G-9, one vein generation is with 115.5 ± 3.1 Ma (G-9 v4) significantly older than the cement age. ~~Based on this~~ In line with our argument based on sample G-10 v1 above, it is plausible that the wall rock was cemented before ~ 115.5 Ma to ~~provide the tensile strength for the~~ allow for a discrete fracture to form. In sample TBK2, ~~deriving~~ derived from the same outcrop as TBK1, the cement has a well-developed ~~coarse~~ equant sparitic to poikilotopic texture (Fig. ~~4e~~ 4d) with crystal sizes that exceed any other analyzed cement sample. This type of texture has ~~also~~ elsewhere been interpreted as evidence for recrystallization (e.g., Saigal and Bjørlykke, 1987; McBride and Milliken, 2006; Worden et al., 2019). ~~A second argument for a cementation zone formation during or immediately after deposition is the age of vein G-10 v1 with 139.3 ± 3.4 Ma, which is close to the upper boundary (age-wise) of the Lindemans Bugt Formation. deposition. In line with our argument based on sample~~ , which, in conjunction with the similar age of the G-9 above, it is unlikely that fractures would form unless the formation was already at least partly cemented cement, gives rise to our similar interpretation for the TBK2 cement, although we cannot fully exclude the possibility of a second cement growth phase.

340

Having established that the cementation zone formed immediately after deposition of the Lindemans Bugt Formation, its maximum formation depth is constrained by the thickness of the remaining part of the unit above the sampled intervals. The litostratigraphic top of the Lindemans Bugt Formation is exposed on a ridge ~ 4500 m away from the Dombjerg Fault (Fig. 2). Using a maximum depositional dip angle of 15° for fault-proximal Lindemans Bugt Formation sedimentary strata (Henstra et al., 2016) allows ~~to interpolate~~ interpolation of the top of this formation towards the fault (Fig. ~~9~~ 11). With this approach, we estimate a maximum thickness of the Lindemans Bugt Formation above sample TBK1cem of ~ 1050 m and above sample G-36cem of ~ 750 m. These thicknesses represent maximum estimates, because the depositional slope angle of the sediments

350

decreases away from the fault. Applying an angle of 10° would for example lower the estimated thickness to 740 m and 530 m above samples TBK1cem and G-36cem, respectively (Fig. 911). Hence, we ~~can confidently~~ estimate that the cementation zone formed at a burial depth of ~ 1000 m or less (compaction not accounted for).

Formation temperatures of the cements can be assessed from the clumped isotope temperatures, although their interpretation needs to be taken with care: Calcite is subject to solid-state reordering of C-O bonds at ambient temperatures $> \sim 100^\circ\text{C}$, which affects the Δ_{47} composition and subsequently deviates the clumped isotope temperature from the initial formation temperature (Passey and Henkes, 2012). For dolomite, solid-state reordering starts at ambient temperatures of $\sim 150^\circ\text{C}$ (Lloyd et al., 2018). It is documented that this resetting is a challenge especially for samples from sedimentary basins, where the rock may have experienced high burial temperatures for long time periods (Henkes et al., 2014; Shenton et al., 2015). For the sedimentary rock of the Lindemans Bugt Formation, the absence of quartz overgrowth in both calcite-cemented and uncemented sediment samples provides a control on the maximum burial temperature. Temperature is a critical factor on the formation of quartz cement, which is known to start at $\sim 70^\circ\text{C}$ and its growth rate increases significantly with increasing temperature (e.g., Walderhaug, 1994; Lander and Walderhaug, 1999; Harwood et al., 2013). ~~while, e.g., silica supply is not regarded as a limiting factor (e.g., Walderhaug, 1996, 2000; Lander et al., 2008; Taylor et al., 2010).~~ Therefore, we argue that the analyzed samples from the Lindemans Bugt Formation have not been subject to temperatures above 100°C and that the clumped isotope temperatures reflect the formation temperatures. However, this excludes samples that were subject to recrystallization, i.e. dissolution and reprecipitation (Eiler, 2011), as well as the basement and fault core samples, whose age/temperature history is not known.

~~Formation temperatures of cements are relatively high when considering their shallow formation depth. Despite being similar in age, the cement samples show a variation in formation temperatures, e.g. $56.6 \pm 10.9^\circ\text{C}$ for G-36cem and $42.0 \pm 10.2^\circ\text{C}$ for TBK1cem. For example, for sample G-36cem, given its formation temperature, a formation depth of 530-750 m (Fig. 9), and an assumed near-surface groundwater temperature of 10°C , a geothermal gradient of $73 \pm 21^\circ\text{C}/\text{km}$ can be calculated, which argues for upward flow of hot fluids along the fault. Localized high geothermal gradients near faults are common and have been reported along other fault systems, such as at the western Svalbard margin (Vanneste et al., 2005), in southern Tuscany/Italy (Bellani et al., 2004), and along the Southern Alpine Fault Zone in New Zealand (Townend et al., 2017). The temperature difference between samples G-36cem (located ~ 300 m away from the fault, and $56.6 \pm 10.9^\circ\text{C}$) and TBK1cem ($42.0 \pm 10.1^\circ\text{C}$), despite being similar in age, for G-36cem, located ~ 1500 m away from the fault (Figs. 9a,b; tables 1, 2). This indicates that fluid circulation and temperature distribution did not occur homogeneously heat flow was heterogeneously distributed in the hanging wall samples, and that highest temperatures are not necessarily found closest to the fault. This may root in permeability variations within the hanging wall deposits, due to e.g. grain size, sorting, or onset of cementation, which may cause local perturbation or channeling of fluid flow and advective heat transfer. Subsequently, upwelling hot fluids along the fault would have adapted variably to the ambient geothermal gradient, depending on their fluid pathway and flow rate. The calculated fluid $\delta^{18}\text{O}_{\text{VSMOW}}$ of the cements allow to assess the fluid source from which the cements precipitated from. In general, the mean marine $\delta^{18}\text{O}_{\text{VSMOW}}$ is regarded as -1‰ for the Cretaceous (e.g., Shackleton and Kennett, 1975; O'Brien et al., 2017). However, it is shown that the marine $\delta^{18}\text{O}$ has likely been inhomogenous in the Early Cretaceous with reported values ranging from -5.3‰ to $+1.5\text{‰}$ (Price and Nunn, 2010; Price et al., 2020), which reflects a similar spread as shown by modern marine~~

$\delta^{18}\text{O}$ (LeGrande and Schmidt, 2006). The fluid $\delta^{18}\text{O}_{\text{VSMOW}}$ values of the cements ~~likely reflect~~, spanning from $-4.3 \pm 1.9 \text{‰}$ to $-0.2 \pm 1.6 \text{‰}$ fit well into this range and likely reflects a marine or potentially a mixed meteoric/marine fluid system, which is unsurprising given the marine deposition environment in the hanging wall basin. ~~The values~~ Henstra et al. (2016) argue for the presence of a delta located to the north of the study area, between the Dombjerg and Thomsenland faults (Fig. 1b), supplied by a large hinterland catchment area. This river system might have provided sufficient inflow of freshwater into the marine hanging wall basin to shift the $\delta^{18}\text{O}$ signature to the more negative values. An additional possibility may be the local influx of meteoric groundwater: the $\delta^{18}\text{O}_{\text{VSMOW}}$ of the cements appear to increase slightly with distance to the fault (Fig. 7e9d) and with the caveat that this observation is based on a limited number of data points, this may be taken to suggest that an influx of meteoric groundwater affected the proximal (near-fault) parts of the hanging wall, but did not access the more proximal hanging wall deposits.

5.2 Timing and formation of calcite veins

The analyzed veins cover a U-Pb age range from 140 to 90 Ma. Only one of these veins (sample G-10 v1) formed during the rift climax stage (Table 1, fig. 68), whereas the majority formed broadly between 125 to 100 Ma in the post-rift stage, accompanied by renewed fracture opening and vein formation between 115 to 90 Ma (Fig. 6). ~~Extensional phases have not been reported for~~ 8). In the Wollaston Forland ~~during the Basin, there is, to our knowledge, no published evidence for tectonic activity in~~ Aptian to Turonian times. However, on northern Hold with Hope, ~80 km south of our study area (Fig. 1), a rift period occurred from end-Valanginian to Middle Albian times with faulting along a series of N–NNE trending normal faults (Whitham et al., 1999). Both vein ages and orientations in our study area fit well with these structures and might therefore correspond to this tectonic phase. On the rift counter-part across the Norway-Greenland Sea, the Lofoten-Vesterålen segment of the Norwegian continental shelf, a rifting phase occurred during the Late Albian (Dalland, 1981; Henstra et al., 2017) and may have a minor contribution to fracturing or fracture reopening. ~~We note however, that with regard to the limited sample number, we cannot fully exclude the possibility of continuous vein formation from the syn-rift into the post-rift.~~

It is also possible that the veins formed in two stages by (i) fracturing during the main rift stage, and ~~ii) fracture cementation~~ (ii) calcite precipitation, in the post-rift stage. However, the vein generation G-10 v1 ~~precipitated-formed~~ at the end of the rift climax (Fig. 68; table 1) showing that the formation conditions were favorable for calcite precipitation in fractures. Hence, it would be reasonable to expect that also other fractures forming during rift climax should be ~~ement-filled~~ calcite-filled, and we therefore consider ~~the above such a~~ two-stage interpretation as less likely, and our preferred interpretation is that the veins formed in their entirety in the post-rift stage. The U-Pb ages of vein samples G-7 (50.1 ± 2.1 Ma) and G-2 (49.4 ± 2.1 Ma) diverge significantly from the main sample suit. These veins closely post-date the extrusion of the plateau basalts covering the Lower Cretaceous late syn-rift Palnatokes Bjerg Formation, ~~which overlies the Lindemans Bugt Formation~~. This event is dated to 56-53 Ma (Larsen et al., 2014) and is related to the onset of continental breakup, which started at the latitude of the Wollaston Forland around 55 Ma (Mjelde et al., 2008; Larsen et al., 2014). Hence, the formation of the veins could be directly related to deformation and uplift following breakup. A second striking difference to the main sample suit is the ~~low~~ fluid

420 $\delta^{18}\text{O}_{\text{VSMOW}}$ value ~~available for G-7, which with -13.7 of -13 ± 1.5 clearly ‰ of sample G-7. It falls well into the global $\delta^{18}\text{O}$ range of -8 ‰ to -20 ‰ for modern meteoric water at 60°N (Terzer et al., 2013), i.e. the paleolatitude of the study area at 50 Ma (Torsvik et al., 2012; van Hinsbergen et al., 2015), and thus most likely~~ indicates a meteoric fluid. We therefore interpret that deformation and, potential, rift shoulder uplift in response to continental breakup (e.g., Wernicke, 1985; Chéry et al., 1992), was responsible for vein formation, which at this time occurred under meteoric conditions.

425 As ~~outlined in the previous chapter suggested above,~~ the clumped isotope temperatures of the hanging wall veins most likely reflect their formation temperatures. These generally lie close to the cement formation temperatures, which may be explained by (i) similar formation depth, (ii) deeper formation depth, but lower geothermal gradient, or (iii) perturbation of fluid flow and advective heat transfer. The latter argument should be valid as the cementation zone has likely created a setting for complex fluid pathways. ~~While, whereas~~ the evolution of the geothermal gradient is difficult to assess, ~~the~~. ~~The~~ burial depth of

430 the analyzed sedimentary rock has increased ~~due to continued deposition of sediments in the hanging wall basin in the after the formation of the cementation zone due to deposition of the~~ late syn-rift ~~and Palnatokes Bjerg Formation and Barremian to Albian~~ post-rift ~~stage (e.g., Surlyk and Korstgård, 2013) sediments (e.g., Nøhr-Hansen, 1993; Surlyk and Korstgård, 2013).~~ Two formation temperatures and ages are obtained of successive precipitation generations from two vein samples, respectively (samples G-10 and G-36; ~~Table table~~ 2, fig. ~~5a7a~~). Both samples yield an increase of formation temperature from old to young

435 ~~vein generation~~ (i.e. from $40.3 \pm 7.1^\circ\text{C}$ ~~at 139.3 ± 3.4 Ma~~ to $61.5 \pm 10.5^\circ\text{C}$ ~~at 90.4 ± 1.5 Ma~~ in sample G-10 and from $36.3 \pm 9.4^\circ\text{C}$ ~~at 122.4 ± 1.3 Ma~~ to $58.2 \pm 14.1^\circ\text{C}$ ~~at 112.0 ± 1.4 Ma~~ in sample G-36), which might indeed reflect an increasing formation depth. ~~However, the possibility persists that the connectivity of fluid pathways may have been in a favorable condition for warmer fluids to circulate through the fractures during the formation of the younger vein generations.~~

For the calcite and dolomite samples from the basement and fault core, it is unclear if the clumped isotope temperatures reflect

440 the original formation temperatures, since an age control is missing. Therefore, these samples may have been partially reset due to ambient temperatures above the threshold of C-O bond reordering of $\sim 100^\circ\text{C}$ for calcite (Passey and Henkes, 2012) and $\sim 150^\circ\text{C}$ for dolomite (Lloyd et al., 2018) in the course of time. ~~For the basement sample G-34, with a~~ ~~The~~ clumped isotope temperature of $128.7 \pm 19.1^\circ\text{C}$ ~~, this possibility may have resulted in a complex mixed signal of original formation, maximum, and cooling temperatures~~ ~~of the basement sample G-34 could therefore reflect the original formation temperature, a maximum ambient temperature, a cooling temperature if the ambient temperature was $>100^\circ\text{C}$ but lower than the calcite formation temperature, or a mixture of these~~.

445 ~~a maximum ambient temperature, a cooling temperature if the ambient temperature was $>100^\circ\text{C}$ but lower than the calcite formation temperature, or a mixture of these~~. For the fault core vein samples, only a partial heating signal may be present as the measured clumped isotope temperatures of both veins are still below the temperature threshold (i.e. a fully reset signal would give a clumped isotope temperature above 100°C for calcite and 150°C for dolomite). Therefore, we are confident that the original formation temperatures of the dolomite and calcite vein samples from the fault core are $\leq 106.5 \pm 11.9^\circ\text{C}$ and

450 $\leq 68.8 \pm 10.9^\circ\text{C}$, respectively. Since both vein networks have a continuous, non-faulted appearance ~~in the outcrop~~ (Fig. ~~3a3e~~), we argue that these veins formed in the late stage of fault activity.

5.3 Origin of calcite components and fluid circulation patterns

One of the main questions around the formation of the cementation zone is the origin of calcium necessary for the calcite cementation. A first likely candidate for a source is calcium from seawater that circulated through the hanging wall ~~elastics~~ succession (Morad, 1998). Such a circulation may be expected to follow general subsurface flow patterns in coastal areas. In such areas, groundwater systems are commonly characterized by ~~saline-marine~~ (i.e. seawater) groundwater circulation that is tidal-, density-, and thermal-driven, and meteoric groundwater flow towards the ocean, driven by the hydraulic head (e.g., Cooper, 1959; Wilson, 2005; Jiao and Post, 2019). ~~Permitted-In~~ the presence of a continuous and undisturbed permeable rock, ~~saline-marine~~ circulation is not restricted to the aquifer underneath the ocean, but extends landward beyond the coastline underneath the body of meteoric groundwater (Fig. ~~10a~~12a). The landward extension of ~~saline-marine~~ groundwater circulation partly depends on the permeability of the aquifer (e.g., Houben et al., 2018; Jiao and Post, 2019). Along the Dombjerg Fault, which defined and delineated the coastline during the rift climax (Surlyk, 1989; Henstra et al., 2016), the footwall is composed of low-permeable crystalline and metamorphic rock with a low fracture and vein density (4 joints + 1 vein per meter; Kristensen et al., 2016). On the other hand, the hanging wall ~~elastics-have~~ succession has distinctly different flow properties than that of low-permeable crystalline basement. Where ~~non-cemented~~uncemented, these deposits are highly porous (Fig. 4e), and therefore presumably permeable allowing for fluid flux at a much larger degree compared to low-fractured crystalline and metamorphic basement rock (e.g., Brace, 1980). Hence, along the Dombjerg Fault, ~~saline-marine~~ fluid circulation should be predominantly restricted to the permeable fault zone and hanging wall ~~elastics-clastic~~ succession (Fig. ~~10b~~12b). Upwelling of warm ~~saline fluids within the elastics-marine~~ fluids along the fault may have been in a favorable condition for the precipitation of calcite from seawater within the vicinity of the fault zone.

A second candidate for a calcium source are Permian carbonate and evaporite deposits underlying the clastic hanging wall rift sediments. While a direct exposure of such rock along the Dombjerg Fault is missing, a Permian carbonate unit is located along the northern section of the Clavering Fault (Fig. 1b; Surlyk, 1978), which forms the southern extension of the Dombjerg Fault. Permian carbonate rock is also exposed at the southern crest of the hanging wall block of the Dombjerg Fault (Fig. 1b; Surlyk, 1978). It may therefore be a reasonable assumption that the Permian succession is also underlying the Lindemans Bugt Formation along the Dombjerg Fault, especially considering that the fault had been active since the Carboniferous (Rotevatn et al., 2018). It has been proposed and modeled elsewhere that surface waters may convect thermally-driven within faults (e.g., López and Smith, 1996; Zhao et al., 2003; Hollis et al., 2017). Such convecting fluids within the Dombjerg Fault may have dissolved the carbonate and transported the solutes into the Lindemans Bugt Formation for the precipitation of calcite.

Other potential sources for calcium can be excluded: No carbonate rock is hosted by the basement and also carbonate deposits in the Palnatokes Bjerg Formation overlying the cementation zone-hosting Lindemans Bugt Formation (i.e. Albrecht Bugt Member; Surlyk and Korstgård, 2013) can be ruled out as a source, since the cementation pre-dates this deposition. Further, dissolution of biogenic carbonate clasts and feldspar alteration appear unlikely ~~for-as~~ a potential internal source. Although biogenic carbonate clasts occur sporadically in some outcrop sections and are visible in a number of thin sections, they do not show signs of dissolution or recrystallization. The degree of feldspar alteration in the sandstone is low and, hence, will not have

provided a significant amount of calcium. Therefore, whether calcium from seawater or dissolved underlying carbonates, it is clear that the calcium must have been introduced into the sediments of the Lindemans Bugt Formation by advective transfer. CO₂ that is acquired for the formation of calcite may have been generated and transported along in the same process. Yet, the negative $\delta^{13}\text{C}_{\text{VPDB}}$ values of the cements hint towards an (additional) internal source: $\delta^{13}\text{C}$ values of calcite cements range from -18.2 ‰ to -9.7 ‰, which are typical values for CO₂ deriving from the degradation of organic matter (e.g., Clark and Fritz, 1997). The high Uranium content of the cements, which allowed the U-Pb calcite dating, also argues for degradation of organic matter, which is commonly bonding Uranium (e.g., Spirakis, 1996; Cumberland et al., 2016). Organic matter is common in the Lindemans Bugt Formation, composing mostly of ammonites, bivalves, belemnites, and transported plant and wood fragments (Pauly et al., 2013; Henstra et al., 2016) and the presence of pyrite in the sediment point towards an organic matter degradation in the sulfate reduction zone (e.g., Jørgensen and Kasten, 2006). Fe and Mn incorporated in the calcite cements and veins is most likely sourced from within the sediments, as their concentration in marine water is generally very low (e.g., Moore and Wade, 2013). Notable is the overall high Fe concentration in the samples, while at the same time being highly variable across the sample suit (Fig. 10, table 3). A major Fe source has likely been biotite, which is frequent in the sandstone, and the formation of pyrite along these grains demonstrates that Fe was released from biotite (Fig. 5). An inhomogeneous distribution of biotite in the sandstone might subsequently be responsible for the spatial variability of Fe concentration in the calcite. The low Sr concentration is more difficult to explain: Sr uptake into calcite is strongly temperature and precipitation rate dependent, i.e. the Sr concentration in calcite decreases with increasing temperature and increases with precipitation rate (e.g., Tang et al., 2008; Swart, 2015). The low Sr concentration may therefore be a result of the elevated precipitation temperature in reference to calcite precipitating at or near the seafloor.

5.4 Permeability of the fault and the cementation zone

Throughout its seismic activity, the Dombjerg Fault was permeable due to repeated fracturing, as commonly assigned to fault zones (e.g., Sibson, 1990) (e.g., Sibson, 1990; Indrevær et al., 2014). The anastomosing dolomite vein network (represented by sample TBK9dol) close to the fault core suggests the fault represented a conduit for vertical (up-fault) fluid migration. It yields a fluid $\delta^{18}\text{O}_{\text{VSMOW}}$ value of $+16.1 \pm 1.6$ (Table 2), which is by far the highest value determined in our sample suit and is indicative for a metamorphic fluid (Sheppard, 1986) that was likely sourced from greater depths. On the contrary, its formation temperature of $\leq 106.5 \pm 11.9^\circ\text{C}$ is not particularly high, which might reflect a moderate flow rate allowing the fluid to adapt to the ambient wall rock temperature.

The younger calcite vein network cutting through the dolomite veins is less pronounced and consists of thinner veins. Its fluid $\delta^{18}\text{O}_{\text{VSMOW}}$ value of -1.8 ± 1.7 ‰ (sample TBK9cal; Table 2) presumably indicates a marine fluid, which may be taken to suggest that the saline-marine groundwater circulation was responsible for its formation. The $\delta^{13}\text{C}$ value of -4.2 ± 0.1 ‰ of this vein differs significantly from hanging wall cements and veins (-23.5 ‰ to -9.7 ‰). Also, the minor element concentration ratio diverges from hanging wall samples with very low Mn and Mg concentrations (Table 3, Fig. 8, Fig. 10). This might

indicate that the ~~saline-marine~~ groundwater circulation, from which the calcite in the fault core fracture network precipitated, was decoupled from groundwater circulation in the hanging wall sediments.

In the hanging wall, the cementation zone will have, once formed, significantly lowered the permeability of the fault-proximal hanging wall sediments, as the carbonate cement reduces the pore space towards 0 %. During progressive formation of the cementation zone and accompanying matrix porosity and permeability loss, fluid circulation becomes increasingly dependent on flowing through fractures developed within this zone. Here, the magnitude of circulation and flow direction is then guided by the connectivity and orientation of the fracture network.

~~A hint towards the degree of fracture connectivity and fluid flow rate is given by the~~ The minor element concentration of cements and veins (Fig. 8-10) may shed light on the fluid flow rate and degree of fracture connectivity in the cementation zone. There is a striking similarity of minor element concentrations between veins and the respective wall rock cement in around half of the analyzed samples. ~~As this pattern is visible in both sample suits of original and recrystallized cement, this pattern seems to be a primary signal,~~ while being variable from sample to sample (Fig. 10, supplementary figure S2). Noteworthy is the compositional difference between samples G-36 and G-38: these samples are located ~2 m apart from each other in the same outcrop, yet especially the Fe concentration of cements and veins varies between the samples, while being similar from respective wall rock cement to vein calcite. While sample G-36 yields an Fe concentration below average, sample G-38 yields the highest Fe concentration of all samples (Fig. 5, table 3). The analyzed 1-inch mount of G-38 hosts a very large quantity of biotite (Fig. 5), which serves as a Fe-source, and could explain this high concentration. If an advective fluid was responsible for both the precipitation of cement and vein calcite, it must have kept a stable minor element composition over ~20 Myr (i.e. ~~reflecting the fluid composition of the initial calcite formation. Hence,~~ the age difference between wall rock cement and vein calcite), which at the same time had to remain highly variable on a local spatial scale. We regard this as unlikely and, therefore, argue that the solute which formed the vein calcite likely was derived from diffusion from the calcite cement into the fracture. Diffusion of mass from local wall rock into a fracture is a common source of vein material and is promoted by, e.g., chemical and pressure gradients between wall rock and fluid-filled fracture (e.g., Oliver and Bons, 2001, and references therein; Bons et al., 2012, and references therein). In addition, calcite is highly susceptible to pressure solution (e.g., Croizé et al., 2010; Toussaint et al., 2018), which may further stimulate the availability of diffusive material. It should be noted, that the possibility of a later equilibrium between cements and vein through solid state diffusion cannot be fully neglected, as this is a process that is poorly understood at low temperatures, though experiments point towards an unlikely mechanism (Fisler and Cygan, 1999; Gorski and Fantle, 2017).

If true, i.e. diffusion being responsible for the vein calcite formation, this indicates very slow advective fluid circulation ~~and a poorly connected fracture network. As the veins are predominantly parallel with a NNE-strike and.~~ Hence, despite being fractured, the effective permeability of the cementation zone remained low, which may root in poor fracture connectivity. The latter may be a reflection of the predominant parallel-striking veins and their near-vertical ~~dip, an interconnection between these veins might have indeed been poor. This emphasizes that the cementation zone was nearly impermeable despite having been subject to fracturing~~ dips, causing limited fracture intersections (Fig. 2).

555

6 Summary and Conclusions

The integration of the analyses of our sample suits sheds light on the fluid flow evolution along the Dombjerg Fault since its syn- to late-rift stage activity. Within the fault, a well-connected fracture network existed at the late stage of fault activity allowing upward flow of metamorphic fluids (Fig. [Ha13a](#)), as evident by the dolomite vein network. At depth, these fluids
560 may have been ~~dragged~~-drawn into the highly fractured fault, where thermal-driven upward flow occurred. Presumably, such networks existed repeatedly in the course of the faults activity. Towards the end of its activity, the fault became sealed to deep fluid circulation, as indicated by the less-pronounced, low-temperature calcite vein network postdating the prominent dolomite vein network.

In the hanging wall, fluid advection followed the common model of groundwater flow in coastal aquifers, with the distinc-
565 tion that thermal-driven upward flow occurred within the sediments along the fault and low-permeable footwall rock (Fig. [10](#), [Hb13b](#), [Hb13c](#)). The cementation zone formed quickly after the deposition of its hosting sediments of the Lindemans Bugt Formation (Fig. [Hb13b](#)), with a formation temperature around 30–70°C at a depth <1 km (Fig. [911](#)). While the calcium for the calcite formation derived from advective fluid transport, CO₂ likely has a component of local formation. Once formed, the cementation zone acts as a low-permeable body and redirects fluid advection in the hanging wall towards the distal parts of the
570 basin, which may in turn be a contributor of the cementation growth farther ~~into the basin~~-away from the fault (Fig. [He13c](#)). Fractures and veins within the cementation zone formed predominantly in the post-rift stage (Fig. [13d](#)) at temperatures around 30–80°C, and might reflect an extensional period during the Aptian to Turonian that has not been identified in the Wollaston Forland before. However, the fracture network did not significantly increase the permeability of the cementation zone. At continental break-up and extrusion of flood basalts in the early Eocene, the marine basin was drained allowing meteoric water to
575 infiltrate the basin and fractures within the cemented clastics (Fig. [Hd13e](#)).

This study highlights the effect of rift faulting on early sediment diagenesis and shows that clastic sediments can become ~~solidified~~-lithified quickly after their deposition. This has an immediate effect on the style of damage zone evolution, as it inhibits the growth of a damage zone featuring deformation bands that would normally be expected to form in porous sediments. Instead, a fracture-dominated damage zone evolves similar to a hard-rock hosted fault. Depending on the degree of fracturing
580 and fracture connectivity within the cementation zone, two separate, decoupled fluid circulation systems may form: one within the uncemented fault-distal sediments and one within the fractured fault zone. This may have an important impact on potential mixing with fluids from under- or overlying reservoirs that are tapped by the fault.

In the management of fault-dependent subsurface aquifers/reservoirs for petroleum, groundwater or geothermal resources, and in CO₂ storage sites, it is important to be aware that in the presence of a fault-proximal cementation zone such as the one
585 studied here, permeability and fluid flow in the vicinity of the fault may be greatly reduced. We therefore suggest, that the possibility of this type of diagenetic seal should be incorporated in fault seal analyses.

Data availability. Replicate level raw data of the clumped isotope analysis are available on the EarthChem database (<https://doi.org/10.26022/IEDA/11160>)

590 *Author contributions.* ES, AR, TBK, SAG, and GAH conducted the field data collection and rock sampling, ANM and ES operated the clumped isotope analysis, AG and RA the U-Pb analysis, and ES the optical and microprobe analyses. All authors were involved in the data analysis and contributed to the manuscript writing.

Competing interests. The authors declare that they have no conflict of interest.

600 *Acknowledgements.* Arild Andresen is thanked for giving support in planning and providing equipment for the field campaign. ~~Enver Alagoz~~ and Sevasti Eleni Modestou [and Enver Alagoz](#) are thanked for support in running the mass spectrometer for the clumped isotope analysis at University of Bergen. Muriel Erambert is thanked for support and setting up the electron microprobe data collection at University of Oslo. [Very constructive reviews by Cathy Hollis and an anonymous reviewer are gratefully acknowledged and helped to improve this contribution.](#) [Roger Soliva is thanked for editorial handling.](#) [Michael Joachimski and Luca Caracciolo are thanked for helpful discussions and Billy Andrews for further comments.](#) The Ministry of Environment and Nature and the Mineral License and Safety Authority of the government of Greenland are thanked for allowing access to the Northeast Greenland National Park for fieldwork conducted under KNNO expedition permit C-18-56 and Scientific Survey License VU-00141. ~~This study~~ [AG and RA would like to acknowledge this paper as FIERCE contribution No. 43. This study was conducted as part of the ARCEX research collaboration and](#) received funding from the ARCEX partners and the Research Council of Norway (grant number 228107).

References

- Bellani, S., Brogi, A., Lazzarotto, A., Liotta, D., and Ranalli, G.: Heat flow, deep temperatures and extensional structures in the Larderello Geothermal Field (Italy): constraints on geothermal fluid flow, *Journal of Volcanology and Geothermal Research*, 132, 15–29, [https://doi.org/10.1016/S0377-0273\(03\)00418-9](https://doi.org/10.1016/S0377-0273(03)00418-9), 2004.
- Bernasconi, S. M., Hu, B., Wacker, U., Fiebig, J., Breitenbach, S. F. M., and Rutz, T.: Background effects on Faraday collectors in gas-source mass spectrometry and implications for clumped isotope measurements, *Rapid communications in mass spectrometry : RCM*, 27, 603–612, <https://doi.org/10.1002/rcm.6490>, 2013.
- Bernasconi, S. M., Müller, I. A., Bergmann, K. D., Breitenbach, S. F. M., Fernandez, A., Hodell, D. A., Jaggi, M., Meckler, A. N., Millan, I., and Ziegler, M.: Reducing Uncertainties in Carbonate Clumped Isotope Analysis Through Consistent Carbonate-Based Standardization, *Geochemistry, Geophysics, Geosystems*, 19, 2895–2914, <https://doi.org/10.1029/2017gc007385>, 2018.
- Bons, P. D., Elburg, M. A., and Gomez-Rivas, E.: A review of the formation of tectonic veins and their microstructures, *Journal of Structural Geology*, 43, 33–62, <https://doi.org/10.1016/j.jsg.2012.07.005>, 2012.
- Brace, W. F.: Permeability of crystalline and argillaceous rocks, *International Journal of Rock Mechanics and Mining Sciences & Geomechanics Abstracts*, 17, 241–251, [https://doi.org/10.1016/0148-9062\(80\)90807-4](https://doi.org/10.1016/0148-9062(80)90807-4), 1980.
- Chéry, J., Lucazeau, F., Daignières, M., and Vilotte, J. P.: Large uplift of rift flanks: A genetic link with lithospheric rigidity?, *Earth and Planetary Science Letters*, 112, 195–211, [https://doi.org/10.1016/0012-821X\(92\)90016-O](https://doi.org/10.1016/0012-821X(92)90016-O), 1992.
- Christiansen, F., Larsen, H., Marcussen, C., Hansen, K., and Krabbe, H.: Uplift study of the Jameson Land basin, East Greenland, *Norsk Geologisk Tidsskrift*, 72, 291–294, 1992.
- Clark, I. D. and Fritz, P.: *Environmental Isotopes in Hydrogeology*, CRC Press, 1997.
- Cooper, H., Kohout, F., Henry, H., and Glover, R.: *Sea Water in Coastal Aquifers*, Tech. rep., US Government Printing Office, Washington, DC, 1964.
- Cooper, H. H.: A hypothesis concerning the dynamic balance of fresh water and salt water in a coastal aquifer, *Journal of Geophysical Research*, 64, 461–467, <https://doi.org/10.1029/JZ064i004p00461>, 1959.
- Corti, G., van Wijk, J., Cloetingh, S., and Morley, C. K.: Tectonic inheritance and continental rift architecture: Numerical and analogue models of the East African Rift system, *Tectonics*, 26, n/a–n/a, <https://doi.org/10.1029/2006TC002086>, 2007.
- Cox, S. F.: Faulting processes at high fluid pressures: An example of fault valve behavior from the Wattle Gully Fault, Victoria, Australia, *Journal of Geophysical Research: Solid Earth*, 100, 12 841–12 859, <https://doi.org/10.1029/95JB00915>, 1995.
- Croizé, D., Renard, F., Bjørlykke, K., and Dysthe, D. K.: Experimental calcite dissolution under stress: Evolution of grain contact microstructure during pressure solution creep, *Journal of Geophysical Research*, 115, <https://doi.org/10.1029/2010JB000869>, 2010.
- Cumberland, S. A., Douglas, G., Grice, K., and Moreau, J. W.: Uranium mobility in organic matter-rich sediments: A review of geological and geochemical processes, *Earth-Science Reviews*, 159, 160–185, <https://doi.org/10.1016/j.earscirev.2016.05.010>, 2016.
- Dalland, A.: Mesozoic sedimentary succession at Andøy, northern Norway, and relation to structural development of the North Atlantic area, in: *Geology of the North Atlantic Borderlands*, pp. 563–584, Canadian Society of Petroleum Geologists Memoir, 1981.
- Dennis, K. J., Affek, H. P., Passey, B. H., Schrag, D. P., and Eiler, J. M.: Defining an absolute reference frame for ‘clumped’ isotope studies of CO₂, *Geochimica et Cosmochimica Acta*, 75, 7117–7131, <https://doi.org/10.1016/j.gca.2011.09.025>, 2011.

- Ebinger, C. J., Jackson, J. A., Foster, A. N., and Hayward, N. J.: Extensional basin geometry and the elastic lithosphere, *Philosophical Transactions of the Royal Society of London. Series A: Mathematical, Physical and Engineering Sciences*, 357, 741–765, <https://doi.org/10.1098/rsta.1999.0351>, 1999.
- 640 Eiler, J. M.: Paleoclimate reconstruction using carbonate clumped isotope thermometry, *Quaternary Science Reviews*, 30, 3575–3588, <https://doi.org/10.1016/j.quascirev.2011.09.001>, 2011.
- Fisler, D. K. and Cygan, R. T.: Diffusion of Ca and Mg in calcite, *American Mineralogist*, 84, 1392–1399, <https://doi.org/10.2138/am-1999-0917>, 1999.
- 645 Gawthorpe, R. L. and Leeder, M. R.: Tectono-sedimentary evolution of active extensional basins, *Basin Research*, 12, 195–218, <https://doi.org/10.1046/j.1365-2117.2000.00121.x>, 2000.
- Gawthorpe, R. L., Fraser, A. J., and Collier, R. E.: Sequence stratigraphy in active extensional basins: implications for the interpretation of ancient basin-fills, *Marine and Petroleum Geology*, 11, 642–658, [https://doi.org/10.1016/0264-8172\(94\)90021-3](https://doi.org/10.1016/0264-8172(94)90021-3), 1994.
- Gorski, C. A. and Fantle, M. S.: Stable mineral recrystallization in low temperature aqueous systems: A critical review, *Geochimica et Cosmochimica Acta*, 198, 439–465, <https://doi.org/10.1016/j.gca.2016.11.013>, 2017.
- 650 Gradstein, F. M., Ogg, J. G., Schmitz, M. D., and Ogg, G. M.: *The geologic time scale 2012*, Elsevier, Amsterdam and Boston, 1st ed. edn., 2012.
- Harwood, J., Aplin, A. C., Fialips, C. I., Iliffe, J. E., Kozdon, R., Ushikubo, T., and Valley, J. W.: Quartz Cementation History of Sandstones Revealed By High-Resolution Sims Oxygen Isotope Analysis, *Journal of Sedimentary Research*, 83, 522–530, <https://doi.org/10.2110/jsr.2013.29>, 2013.
- 655 Henkes, G. A., Passey, B. H., Grossman, E. L., Shenton, B. J., Pérez-Huerta, A., and Yancey, T. E.: Temperature limits for preservation of primary calcite clumped isotope paleotemperatures, *Geochimica et Cosmochimica Acta*, 139, 362–382, <https://doi.org/10.1016/j.gca.2014.04.040>, 2014.
- Henriksen, N.: Caledonian Orogen East Greenland 70–82 N. Geological map 1:100000, Tech. rep., GEUS, Copenhagen, Greenland, 2003.
- 660 Henstra, G. A., Grundvåg, S.-A., Johannessen, E. P., Kristensen, T. B., Midtkandal, I., Nystuen, J. P., Rotevatn, A., Surlyk, F., Sæther, T., and Windelstad, J.: Depositional processes and stratigraphic architecture within a coarse-grained rift-margin turbidite system: The Wollaston Forland Group, east Greenland, *Marine and Petroleum Geology*, 76, 187–209, <https://doi.org/10.1016/j.marpetgeo.2016.05.018>, 2016.
- Henstra, G. A., Gawthorpe, R. L., Helland-Hansen, W., Ravnås, R., and Rotevatn, A.: Depositional systems in multiphase rifts: seismic case study from the Lofoten margin, Norway, *Basin Research*, 29, 447–469, <https://doi.org/10.1111/bre.12183>, 2017.
- 665 Hollinsworth, A. D., Koehn, D., Dempster, T. J., and Aanyu, K.: Structural controls on the interaction between basin fluids and a rift flank fault: Constraints from the Bwamba Fault, East African Rift, *Journal of Structural Geology*, 118, 236–249, <https://doi.org/10.1016/j.jsg.2018.10.012>, 2019.
- Hollis, C., Bastesen, E., Boyce, A., Corlett, H., Gawthorpe, R., Hirani, J., Rotevatn, A., and Whitaker, F.: Fault-controlled dolomitization in a rift basin, *Geology*, 45, 219–222, <https://doi.org/10.1130/G38s394.1>, 2017.
- 670 Horita, J.: Oxygen and carbon isotope fractionation in the system dolomite–water–CO₂ to elevated temperatures, *Geochimica et Cosmochimica Acta*, 129, 111–124, <https://doi.org/10.1016/j.gca.2013.12.027>, 2014.
- Houben, G. J., Stoeckl, L., Mariner, K. E., and Choudhury, A. S.: The influence of heterogeneity on coastal groundwater flow - physical and numerical modeling of fringing reefs, dykes and structured conductivity fields, *Advances in Water Resources*, 113, 155–166, <https://doi.org/10.1016/j.advwatres.2017.11.024>, 2018.

- 675 Indrevær, K., Stunitz, H., and Bergh, S. G.: On Palaeozoic–Mesozoic brittle normal faults along the SW Barents Sea margin: fault processes and implications for basement permeability and margin evolution, *Journal of the Geological Society*, 171, 831–846, <https://doi.org/10.1144/jgs2014-018>, 2014.
- Jiao, J. and Post, V.: *Coastal hydrogeology*, Cambridge University Press, Cambridge, 2019.
- John, C. M. and Bowen, D.: Community software for challenging isotope analysis: First applications of 'Easotope' to clumped isotopes, 680 *Rapid communications in mass spectrometry* : RCM, 30, 2285–2300, <https://doi.org/10.1002/rcm.7720>, 2016.
- Jørgensen, B. B. and Kasten, S.: Sulfur Cycling and Methane Oxidation, in: *Marine Geochemistry*, edited by Schulz, H. D. and Zabel, M., pp. 271–309, Springer-Verlag Berlin Heidelberg, Berlin, Heidelberg, https://doi.org/10.1007/3-540-32144-6_8, 2006.
- Karolytè, R., Johnson, G., Yielding, G., and Gilfillan, S. M.: Fault seal modelling – the influence of fluid properties on fault sealing capacity in hydrocarbon and CO₂ systems, *Petroleum Geoscience*, pp. petgeo2019–126, <https://doi.org/10.1144/petgeo2019-126>, 2020.
- 685 Kele, S., Breitenbach, S. F., Capezzuoli, E., Meckler, A. N., Ziegler, M., Millan, I. M., Kluge, T., Deák, J., Hanselmann, K., John, C. M., Yan, H., Liu, Z., and Bernasconi, S. M.: Temperature dependence of oxygen- and clumped isotope fractionation in carbonates: A study of travertines and tufas in the 6–95°C temperature range, *Geochimica et Cosmochimica Acta*, 168, 172–192, <https://doi.org/10.1016/j.gca.2015.06.032>, 2015.
- Kim, S.-T. and O'Neil, J. R.: Equilibrium and nonequilibrium oxygen isotope effects in synthetic carbonates, *Geochimica et Cosmochimica* 690 *Acta*, 61, 3461–3475, [https://doi.org/10.1016/S0016-7037\(97\)00169-5](https://doi.org/10.1016/S0016-7037(97)00169-5), 1997.
- Kristensen, T. B., Rotevatn, A., Peacock, D. C., Henstra, G. A., Midtkandal, I., and Grundvåg, S.-A.: Structure and flow properties of syn-rift border faults: The interplay between fault damage and fault-related chemical alteration (Dombjerg Fault, Wollaston Forland, NE Greenland), *Journal of Structural Geology*, 92, 99–115, <https://doi.org/10.1016/j.jsg.2016.09.012>, 2016.
- Lander, R. H. and Walderhaug, O.: Predicting Porosity through Simulating Sandstone Compaction and Quartz Cementation, *AAPG Bulletin*, 695 pp. 433–449, <https://doi.org/10.1306/00AA9BC4-1730-11D7-8645000102C1865D>, 1999.
- Lander, R. H., Larese, R. E., and Bonnell, L. M.: Toward more accurate quartz cement models: The importance of euhedral versus noneuhedral growth rates, *AAPG Bulletin*, 92, 1537–1563, <https://doi.org/10.1306/07160808037>, 2008.
- Larsen, L. M. and Watt, W. S.: Episodic volcanism during break-up of the North Atlantic: evidence from the East Greenland plateau basalts, *Earth and Planetary Science Letters*, 73, 105–116, [https://doi.org/10.1016/0012-821X\(85\)90038-X](https://doi.org/10.1016/0012-821X(85)90038-X), 1985.
- 700 Larsen, L. M., Pedersen, A. K., Tegner, C., and Duncan, R. A.: Eocene to Miocene igneous activity in NE Greenland: northward younging of magmatism along the East Greenland margin, *Journal of the Geological Society*, 171, 539–553, <https://doi.org/10.1144/jgs2013-118>, 2014.
- LeGrande, A. N. and Schmidt, G. A.: Global gridded data set of the oxygen isotopic composition in seawater, *Geophysical Research Letters*, 33, <https://doi.org/10.1029/2006GL026011>, 2006.
- 705 Lloyd, M. K., Ryb, U., and Eiler, J. M.: Experimental calibration of clumped isotope reordering in dolomite, *Geochimica et Cosmochimica Acta*, 242, 1–20, <https://doi.org/10.1016/j.gca.2018.08.036>, 2018.
- López, D. L. and Smith, L.: Fluid flow in fault zones: Influence of hydraulic anisotropy and heterogeneity on the fluid flow and heat transfer regime, *Water Resources Research*, 32, 3227–3235, <https://doi.org/10.1029/96WR02101>, 1996.
- McBride, E. F. and Milliken, K. L.: Giant calcite-cemented concretions, Dakota Formation, central Kansas, USA, *Sedimentology*, 53, 1161–710 1179, <https://doi.org/10.1111/j.1365-3091.2006.00813.x>, 2006.

- Meckler, A. N., Ziegler, M., Millán, M. I., Breitenbach, S. F. M., and Bernasconi, S. M.: Long-term performance of the Kiel carbonate device with a new correction scheme for clumped isotope measurements, *Rapid communications in mass spectrometry* : RCM, 28, 1705–1715, <https://doi.org/10.1002/rcm.6949>, 2014.
- 715 Meinicke, N., Ho, S. L., Hannisdal, B., Nürnberg, D., Tripathi, A., Schiebel, R., and Meckler, A. N.: A robust calibration of the clumped isotopes to temperature relationship for foraminifers, *Geochimica et Cosmochimica Acta*, 270, 160–183, <https://doi.org/10.1016/j.gca.2019.11.022>, 2020.
- Mitchell, T. M. and Faulkner, D. R.: Towards quantifying the matrix permeability of fault damage zones in low porosity rocks, *Earth and Planetary Science Letters*, 339–340, 24–31, <https://doi.org/10.1016/j.epsl.2012.05.014>, 2012.
- Mjelde, R., Breivik, A. J., Raum, T., Mittelstaedt, E., Ito, G., and Faleide, J. I.: Magmatic and tectonic evolution of the North Atlantic, *Journal of the Geological Society*, 165, 31–42, <https://doi.org/10.1144/0016-76492007-018>, 2008.
- 720 Moore, C. H. and Wade, W. J.: Carbonate reservoirs: Porosity and diagenesis in a sequence stratigraphic framework, vol. 67 of *Developments in sedimentology*, Elsevier, Amsterdam, 2. ed. edn., 2013.
- Morad, S., ed.: Carbonate cementation in sandstones: Distribution patterns and geochemical evolution, vol. 26 of *The international association of sedimentologists special publication*, Blackwell Science, [S.l.], 1998.
- 725 Morley, C. K.: Developments in the structural geology of rifts over the last decade and their impact on hydrocarbon exploration, Geological Society, London, Special Publications, 80, 1–32, <https://doi.org/10.1144/GSL.SP.1995.080.01.01>, 1995.
- Müller, I. A., Rodriguez-Blanco, J. D., Storck, J.-C., do Nascimento, G. S., Bontognali, T. R., Vasconcelos, C., Benning, L. G., and Bernasconi, S. M.: Calibration of the oxygen and clumped isotope thermometers for (proto-)dolomite based on synthetic and natural carbonates, *Chemical Geology*, 525, 1–17, <https://doi.org/10.1016/j.chemgeo.2019.07.014>, 2019.
- 730 Nøhr-Hansen, H.: Dinoflagellate cyst stratigraphy of the Barremian to Albian, Lower Cretaceous, North-East Greenland, *Grønlands Geologiske Undersøgelse*, pp. 1–171, 1993.
- O'Brien, C. L., Robinson, S. A., Pancost, R. D., Sinninghe Damsté, J. S., Schouten, S., Lunt, D. J., Alsenz, H., Bornemann, A., Bottini, C., Brassell, S. C., Farnsworth, A., Forster, A., Huber, B. T., Inglis, G. N., Jenkyns, H. C., Linnert, C., Littler, K., Markwick, P., McAnena, A., Mutterlose, J., Naafs, B. D. A., Püttmann, W., Sluijs, A., van Helmond, N. A., Vellekoop, J., Wagner, T., and Wrobel, N. E.: Cretaceous
- 735 sea-surface temperature evolution: Constraints from TEX 86 and planktonic foraminiferal oxygen isotopes, *Earth-Science Reviews*, 172, 224–247, <https://doi.org/10.1016/j.earscirev.2017.07.012>, 2017.
- Oliver, N. H. S. and Bons, P. D.: Mechanisms of fluid flow and fluid-rock interaction in fossil metamorphic hydrothermal systems inferred from vein-wallrock patterns, geometry and microstructure, *Geofluids*, 1, 137–162, <https://doi.org/10.1046/j.1468-8123.2001.00013.x>, 2001.
- 740 Passey, B. H. and Henkes, G. A.: Carbonate clumped isotope bond reordering and geospeedometry, *Earth and Planetary Science Letters*, 351–352, 223–236, <https://doi.org/10.1016/j.epsl.2012.07.021>, 2012.
- Pauly, S., Mutterlose, J., and Alsen, P.: Depositional environments of Lower Cretaceous (Ryazanian–Barremian) sediments from Wollaston Forland and Kuhn Ø, North-East Greenland., *Bulletin of the Geological Society of Denmark*, 61, 19–36, 2013.
- Pei, Y., Paton, D. A., Knipe, R. J., and Wu, K.: A review of fault sealing behaviour and its evaluation in siliciclastic rocks, *Earth-Science Reviews*, 150, 121–138, <https://doi.org/10.1016/j.earscirev.2015.07.011>, 2015.
- 745 Phillips, T. B., Jackson, C. A.-L., Bell, R. E., Duffy, O. B., and Fossen, H.: Reactivation of intrabasement structures during rifting: A case study from offshore southern Norway, *Journal of Structural Geology*, 91, 54–73, <https://doi.org/10.1016/j.jsg.2016.08.008>, 2016.

- Piasecki, A., Bernasconi, S. M., Grauel, A.-L., Hannisdal, B., Ho, S. L., Leutert, T. J., Marchitto, T. M., Meinicke, N., Tisserand, A., and Meckler, N.: Application of Clumped Isotope Thermometry to Benthic Foraminifera, *Geochemistry, Geophysics, Geosystems*, 20, 2082–2090, <https://doi.org/10.1029/2018GC007961>, 2019.
- 750 Price, G. D. and Nunn, E. V.: Valanginian isotope variation in glendonites and belemnites from Arctic Svalbard: Transient glacial temperatures during the Cretaceous greenhouse, *Geology*, 38, 251–254, <https://doi.org/10.1130/G30593.1>, 2010.
- Price, G. D., Bajnai, D., and Fiebig, J.: Carbonate clumped isotope evidence for latitudinal seawater temperature gradients and the oxygen isotope composition of Early Cretaceous seas, *Palaeogeography, Palaeoclimatology, Palaeoecology*, 552, 109–177, <https://doi.org/10.1016/j.palaeo.2020.109777>, 2020.
- 755 Prosser, S.: Rift-related linked depositional systems and their seismic expression, Geological Society, London, Special Publications, 71, 35–66, <https://doi.org/10.1144/GSL.SP.1993.071.01.03>, 1993.
- Rawling, G. C., Goodwin, L. B., and Wilson, J. L.: Internal architecture, permeability structure, and hydrologic significance of contrasting fault-zone types, *Geology*, 29, 43, [https://doi.org/10.1130/0091-7613\(2001\)029<0043:IAPSAH>2.0.CO;2](https://doi.org/10.1130/0091-7613(2001)029<0043:IAPSAH>2.0.CO;2), 2001.
- 760 Ring, U.: The influence of preexisting structure on the evolution of the Cenozoic Malawi rift (East African rift system), *Tectonics*, 13, 313–326, <https://doi.org/10.1029/93TC03188>, 1994.
- Rotevatn, A., Kristensen, T. B., Ksienzyk, A. K., Wemmer, K., Henstra, G. A., Midtkandal, I., Grundvåg, S.-A., and Andresen, A.: Structural Inheritance and Rapid Rift-Length Establishment in a Multiphase Rift: The East Greenland Rift System and its Caledonian Orogenic Ancestry, *Tectonics*, 37, 1858–1875, <https://doi.org/10.1029/2018TC005018>, 2018.
- 765 Saigal, G. C. and Bjørlykke, K.: Carbonate cements in clastic reservoir rocks from offshore Norway—relationships between isotopic composition, textural development and burial depth, Geological Society, London, Special Publications, 36, 313–324, <https://doi.org/10.1144/GSL.SP.1987.036.01.22>, 1987.
- Salomon, E., Koehn, D., and Passchier, C.: Brittle reactivation of ductile shear zones in NW Namibia in relation to South Atlantic rifting, *Tectonics*, 34, 70–85, <https://doi.org/10.1002/2014TC003728>, 2015.
- 770 Shackleton, N. J. and Kennett, J. P.: Paleotemperature history of the Cenozoic and the initiation of Antarctic glaciation: oxygen and carbon isotopic analyses in DSDP Sites 277, 279 and 281, Initial Reports of Deep Sea Drilling Project, 29, 743–755, 1975.
- Sharp, I. R., Gawthorpe, R. L., Underhill, J. R., and Gupta, S.: Fault-propagation folding in extensional settings: Examples of structural style and synrift sedimentary response from the Suez rift, Sinai, Egypt, *Geological Society of America Bulletin*, 112, 1877–1899, [https://doi.org/10.1130/0016-7606\(2000\)112<1877:FPFIES>2.0.CO;2](https://doi.org/10.1130/0016-7606(2000)112<1877:FPFIES>2.0.CO;2), 2000.
- 775 Sheldon, H. A. and Mickelthwaite, S.: Damage and permeability around faults: Implications for mineralization, *Geology*, 35, 903, <https://doi.org/10.1130/G23860A.1>, 2007.
- Shenton, B. J., Grossman, E. L., Passey, B. H., Henkes, G. A., Becker, T. P., Laya, J. C., Perez-Huerta, A., Becker, S. P., and Lawson, M.: Clumped isotope thermometry in deeply buried sedimentary carbonates: The effects of bond reordering and recrystallization, *Geological Society of America Bulletin*, p. B31169.1, <https://doi.org/10.1130/B31169.1>, 2015.
- 780 Sheppard, S. M. F.: Characterization and isotopic variations in natural waters, *Reviews in Mineralogy and Geochemistry*, 16, 165–183, 1986.
- Sibson, R. H.: Conditions for fault-valve behaviour, Geological Society, London, Special Publications, 54, 15–28, <https://doi.org/10.1144/GSL.SP.1990.054.01.02>, 1990.
- Sibson, R. H., Moore, J. M. M., and Rankin, A. H.: Seismic pumping—a hydrothermal fluid transport mechanism, *Journal of the Geological Society*, 131, 653–659, <https://doi.org/10.1144/gsjgs.131.6.0653>, 1975.

- 785 Smeraglia, L., Berra, F., Billi, A., Boschi, C., Carminati, E., and Doglioni, C.: Origin and role of fluids involved in the seismic cycle of extensional faults in carbonate rocks, *Earth and Planetary Science Letters*, 450, 292–305, <https://doi.org/10.1016/j.epsl.2016.06.042>, 2016.
- Sperrevik, S., Gillespie, P. A., Fisher, Q. J., Halvorsen, T., and Knipe, R. J.: Empirical estimation of fault rock properties, in: *Hydrocarbon seal quantification*, edited by Hunsdale, R. and Koestler, A., vol. 11 of *Special publication / Norwegian Petroleum Society*, pp. 109–125, Elsevier, Amsterdam [u.a.], [https://doi.org/10.1016/S0928-8937\(02\)80010-8](https://doi.org/10.1016/S0928-8937(02)80010-8), 2002.
- 790 Spirakis, C. S.: The roles of organic matter in the formation of uranium deposits in sedimentary rocks, *Ore Geology Reviews*, 11, 53–69, [https://doi.org/10.1016/0169-1368\(95\)00015-1](https://doi.org/10.1016/0169-1368(95)00015-1), 1996.
- Stemmerik, L., Vigran, J. O., and Piasecki, S.: Dating of late Paleozoic rifting events in the North Atlantic: New biostratigraphic data from the uppermost Devonian and Carboniferous of East Greenland, *Geology*, 19, 218, [https://doi.org/10.1130/0091-7613\(1991\)019<0218:DOLPRE>2.3.CO;2](https://doi.org/10.1130/0091-7613(1991)019<0218:DOLPRE>2.3.CO;2), 1991.
- 795 Surlyk, F.: Submarine fan sedimentation along fault scarps on tilted fault blocks (Jurassic-Cretaceous boundary, East Greenland), vol. no. 128 of *Bulletin / Grønlands Geologiske Undersøgelse*, Grønlands Geologiske Undersøgelse, Copenhagen, 1978.
- Surlyk, F.: Fan-delta to submarine fan conglomerates of the Volgian-Valanginian Wollaston Foreland Group, East Greenland., *Sedimentology of gravels and conglomerates*, in: *Sedimentology of Gravels and Conglomerates*, vol. 10, pp. 359–382, Canadian Society of Petroleum Geology, 1984.
- 800 Surlyk, F.: Mid-Mesozoic syn-rift turbidite systems: controls and predictions, in: *Correlation in Hydrocarbon Exploration*, edited by Collinson, J. D., pp. 231–241, Springer Netherlands, Dordrecht, https://doi.org/10.1007/978-94-009-1149-9_18, 1989.
- Surlyk, F.: Timing, style and sedimentary evolution of Late Palaeozoic-Mesozoic extensional basins of East Greenland, *Geological Society, London, Special Publications*, 55, 107–125, <https://doi.org/10.1144/GSL.SP.1990.055.01.05>, 1990.
- 805 Surlyk, F.: The Jurassic of East Greenland: a sedimentary record of thermal subsidence, onset and culmination of rifting, *Geological Survey of Denmark and Greenland Bulletin*, 1, 659–722, 2003.
- Surlyk, F. and Korstgård, J.: Crestal unconformities on an exposed Jurassic tilted fault block, Wollaston Forland, East Greenland as an analogue for buried hydrocarbon traps, *Marine and Petroleum Geology*, 44, 82–95, <https://doi.org/10.1016/j.marpetgeo.2013.03.009>, 2013.
- Surlyk, F., Hurst, J. M., Piasecki, S., Rolle, F., Scholle, P. A., Stemmerik, L., and Thomsen, E.: The Permian of the Western Margin of the Greenland Sea—A Future Exploration Target, in: *Future Petroleum Provinces of the World*, pp. 629–659, American Association of Petroleum Geologists, <https://doi.org/10.1306/M40454C30>, 1986.
- 810 Surlyk, F., Noe-Nygaard, N., and Dam, G.: High and low resolution sequence stratigraphy in lithological prediction—examples from the Mesozoic around the northern North Atlantic, *Geological Society, London, Petroleum Geology Conference series*, 4, 199–214, <https://doi.org/10.1144/0040199>, 1993.
- 815 Swart, P. K.: The geochemistry of carbonate diagenesis: The past, present and future, *Sedimentology*, 62, 1233–1304, <https://doi.org/10.1111/sed.12205>, 2015.
- Tang, J., Köhler, S. J., and Dietzel, M.: Sr²⁺/Ca²⁺ and 44Ca/40Ca fractionation during inorganic calcite formation: I. Sr incorporation, *Geochimica et Cosmochimica Acta*, 72, 3718–3732, <https://doi.org/10.1016/j.gca.2008.05.031>, 2008.
- Taylor, T. R., Giles, M. R., Hathon, L. A., Diggs, T. N., Braunsdorf, N. R., Birbiglia, G. V., Kittridge, M. G., Macaulay, C. I., and Espejo, I. S.: Sandstone diagenesis and reservoir quality prediction: Models, myths, and reality, *AAPG Bulletin*, 94, 1093–1132, <https://doi.org/10.1306/04211009123>, 2010.
- 820

- Terzer, S., Wassenaar, L. I., Araguás-Araguás, L. J., and Aggarwal, P. K.: Global isoscapes for $\delta^{18}\text{O}$ and $\delta^2\text{H}$ in precipitation: improved prediction using regionalized climatic regression models, *Hydrology and Earth System Sciences*, 17, 4713–4728, <https://doi.org/10.5194/hess-17-4713-2013>, 2013.
- 825 Thomson, K., Green, P. F., Whitham, A. G., Price, S. P., and Underhill, J. R.: New constraints on the thermal history of North-East Greenland from apatite fission-track analysis, *Geological Society of America Bulletin*, 111, 1054–1068, [https://doi.org/10.1130/0016-7606\(1999\)111<1054:NCOTTH>2.3.CO;2](https://doi.org/10.1130/0016-7606(1999)111<1054:NCOTTH>2.3.CO;2), 1999.
- Torsvik, T. H., van der Voo, R., Preeden, U., Mac Niocaill, C., Steinberger, B., Doubrovine, P. V., van Hinsbergen, D. J., Domeier, M., Gaina, C., Tohver, E., Meert, J. G., McCausland, P. J., and Cocks, L. R. M.: Phanerozoic polar wander, palaeogeography and dynamics, *Earth-Science Reviews*, 114, 325–368, <https://doi.org/10.1016/j.earscirev.2012.06.007>, 2012.
- 830 Toussaint, R., Aharonov, E., Koehn, D., Gratier, J.-P., Ebner, M., Baud, P., Rolland, A., and Renard, F.: Stylolites: A review, *Journal of Structural Geology*, 114, 163–195, <https://doi.org/10.1016/j.jsg.2018.05.003>, 2018.
- Townend, J., Sutherland, R., Toy, V. G., Doan, M.-L., Célérier, B., Massiot, C., Coussens, J., Jeppson, T., Janku-Capova, L., Remaud, L., Upton, P., Schmitt, D. R., Pezard, P., Williams, J., Allen, M. J., Baratin, L.-M., Barth, N., Becroft, L., Boese, C. M., Boulton, C., Broderick, N., Carpenter, B., Chamberlain, C. J., Cooper, A., Coutts, A., Cox, S. C., Craw, L., Eccles, J. D., Faulkner, D., Grieve, J., Grochowski, J., Gulley, A., Hartog, A., Henry, G., Howarth, J., Jacobs, K., Kato, N., Keys, S., Kirilova, M., Kometani, Y., Langridge, R., Lin, W., Little, T., Lukacs, A., Mallyon, D., Mariani, E., Mathewson, L., Melosh, B., Menzies, C., Moore, J., Morales, L., Mori, H., Niemeijer, A., Nishikawa, O., Nitsch, O., Paris, J., Prior, D. J., Sauer, K., Savage, M. K., Schleicher, A., Shigematsu, N., Taylor-Offord, S., Teagle, D., Tobin, H., Valdez, R., Weaver, K., Wiersberg, T., and Zimmer, M.: Petrophysical, Geochemical, and Hydrological Evidence for Extensive Fracture-Mediated Fluid and Heat Transport in the Alpine Fault’s Hanging-Wall Damage Zone, *Geochemistry, Geophysics, Geosystems*, 18, 4709–4732, <https://doi.org/10.1002/2017GC007202>, 2017.
- 840 van Hinsbergen, D. J. J., de Groot, L. V., van Schaik, S. J., Spakman, W., Bijl, P. K., Sluijs, A., Langereis, C. G., and Brinkhuis, H.: A Paleolatitude Calculator for Paleoclimate Studies, *PloS one*, 10, e0126946, <https://doi.org/10.1371/journal.pone.0126946>, 2015.
- Vanneste, M., Guidard, S., and Mienert, J.: Bottom-simulating reflections and geothermal gradients across the western Svalbard margin, *Terra Nova*, 17, 510–516, <https://doi.org/10.1111/j.1365-3121.2005.00643.x>, 2005.
- 845 Vermeesch, P., Resentini, A., and Garzanti, E.: An R package for statistical provenance analysis, *Sedimentary Geology*, 336, 14–25, <https://doi.org/10.1016/j.sedgeo.2016.01.009>, 2016.
- Walderhaug, O.: Precipitation rates for quartz cement in sandstones determined by fluid-inclusion microthermometry and temperature-history modeling, *Journal of Sedimentary Research*, 64, 324–333, <https://doi.org/10.2110/jsr.64.324>, 1994.
- 850 Walderhaug, O.: Kinetic Modeling of Quartz Cementation and Porosity Loss in Deeply Buried Sandstone Reservoirs, *Geology*, 80, <https://doi.org/10.1306/64ED88A4-1724-11D7-8645000102C1865D>, 1996.
- Walderhaug, O.: Modeling Quartz Cementation and Porosity in Middle Jurassic Brent Group Sandstones of the Kvitebjørn Field, Northern North Sea, *Geology*, 84, <https://doi.org/10.1306/A9673E96-1738-11D7-8645000102C1865D>, 2000.
- Wernicke, B.: Uniform-sense normal simple shear of the continental lithosphere, *Canadian Journal of Earth Sciences*, 22, 108–125, <https://doi.org/10.1139/e85-009>, 1985.
- 855 Whipp, P. S., Jackson, C. A.-L., Gawthorpe, R. L., Dreyer, T., and Quinn, D.: Normal fault array evolution above a reactivated rift fabric; a subsurface example from the northern Horda Platform, Norwegian North Sea, *Basin Research*, 26, 523–549, <https://doi.org/10.1111/bre.12050>, 2014.

- Whitham, A. G., Price, S. P., Koraini, A. M., and Kelly, S. R. A.: Cretaceous (post-Valanginian) sedimentation and rift events in NE Greenland (71–77°N), Geological Society, London, Petroleum Geology Conference series, 5, 325–336, <https://doi.org/10.1144/0050325>, 1999.
- 860 Wibberley, C. A. and Shimamoto, T.: Internal structure and permeability of major strike-slip fault zones: the Median Tectonic Line in Mie Prefecture, Southwest Japan, *Journal of Structural Geology*, 25, 59–78, [https://doi.org/10.1016/S0191-8141\(02\)00014-7](https://doi.org/10.1016/S0191-8141(02)00014-7), 2003.
- Williams, R. T., Goodwin, L. B., Mozley, P. S., Beard, B. L., and Johnson, C. M.: Tectonic controls on fault zone flow pathways in the Rio Grande rift, New Mexico, USA, *Geology*, 43, 723–726, <https://doi.org/10.1130/G36799.1>, 2015.
- 865 Wilson, A. M.: Fresh and saline groundwater discharge to the ocean: A regional perspective, *Water Resources Research*, 41, 257, <https://doi.org/10.1029/2004WR003399>, 2005.
- Worden, R. H., Morrall, G. T., Kelly, S., Mc Ardle, P., and Barshep, D. V.: A renewed look at calcite cement in marine-deltaic sandstones: the Brent Reservoir, Heather Field, northern North Sea, UK, Geological Society, London, Special Publications, 2, SP484–2018–43, <https://doi.org/10.1144/SP484-2018-43>, 2019.
- 870 Yielding, G., Bretan, P., and Freeman, B.: Fault seal calibration: a brief review, Geological Society, London, Special Publications, 347, 243–255, <https://doi.org/10.1144/SP347.14>, 2010.
- Zhao, C., Hobbs, B. E., Mühlhaus, H. B., Ord, A., and Lin, G.: Convective instability of 3-D fluid-saturated geological fault zones heated from below, *Geophysical Journal International*, 155, 213–220, <https://doi.org/10.1046/j.1365-246X.2003.02032.x>, 2003.

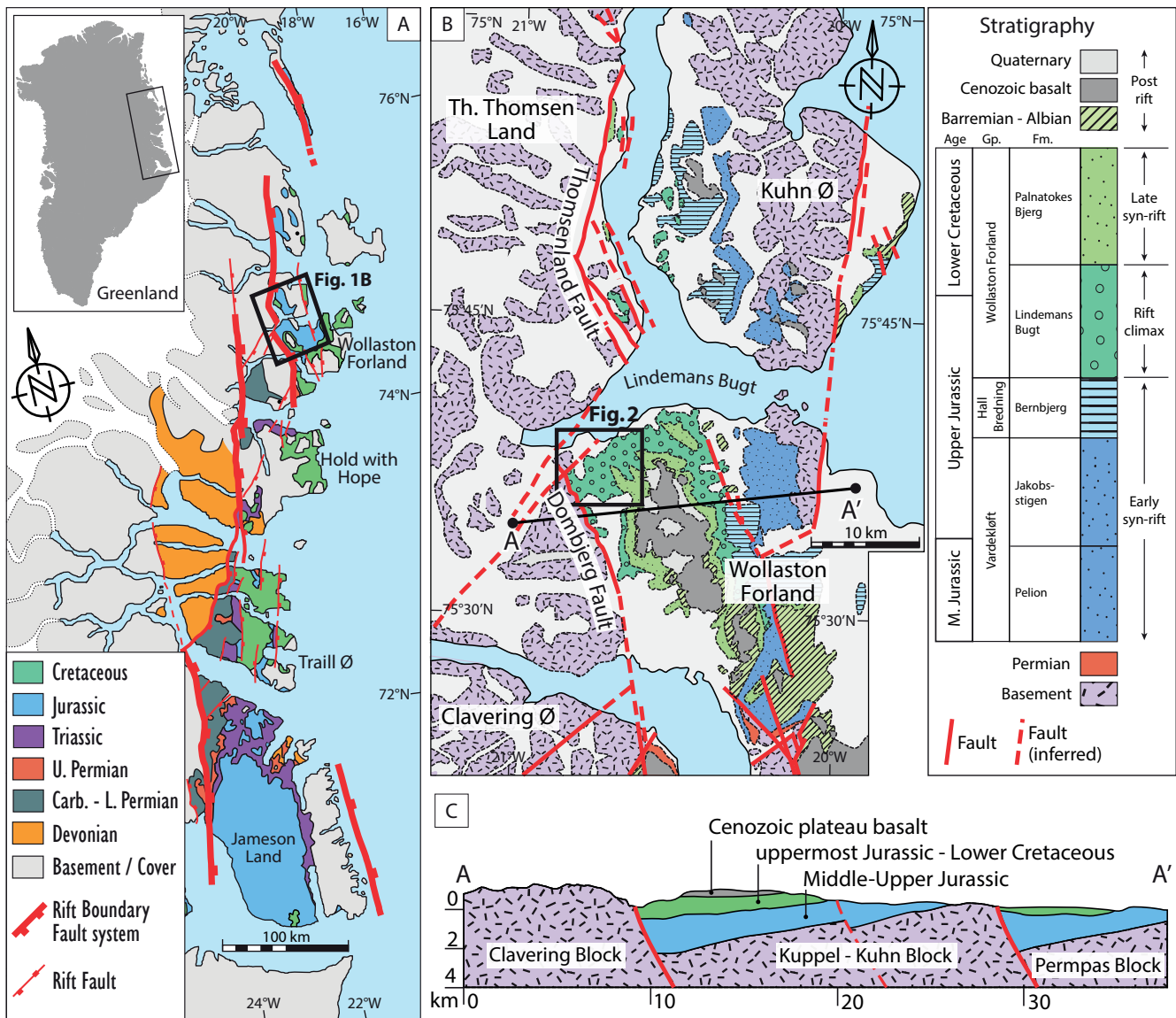


Figure 1. (a) Regional geological map of NE Greenland with right-stepping rift boundary fault system separating Devonian-Jurassic sedimentary basins from Caledonian basement. (b) Geological map of the Wollaston Forland and its surrounding. (c) Geological cross section of the Wollaston Forland Basin (see (b) for location). Modified after Rotevatn et al. (2018), based on Surlyk et al. (1993), Surlyk (2003), Henriksen (2003), Surlyk and Korstgård (2013), and Henstra et al. (2016).

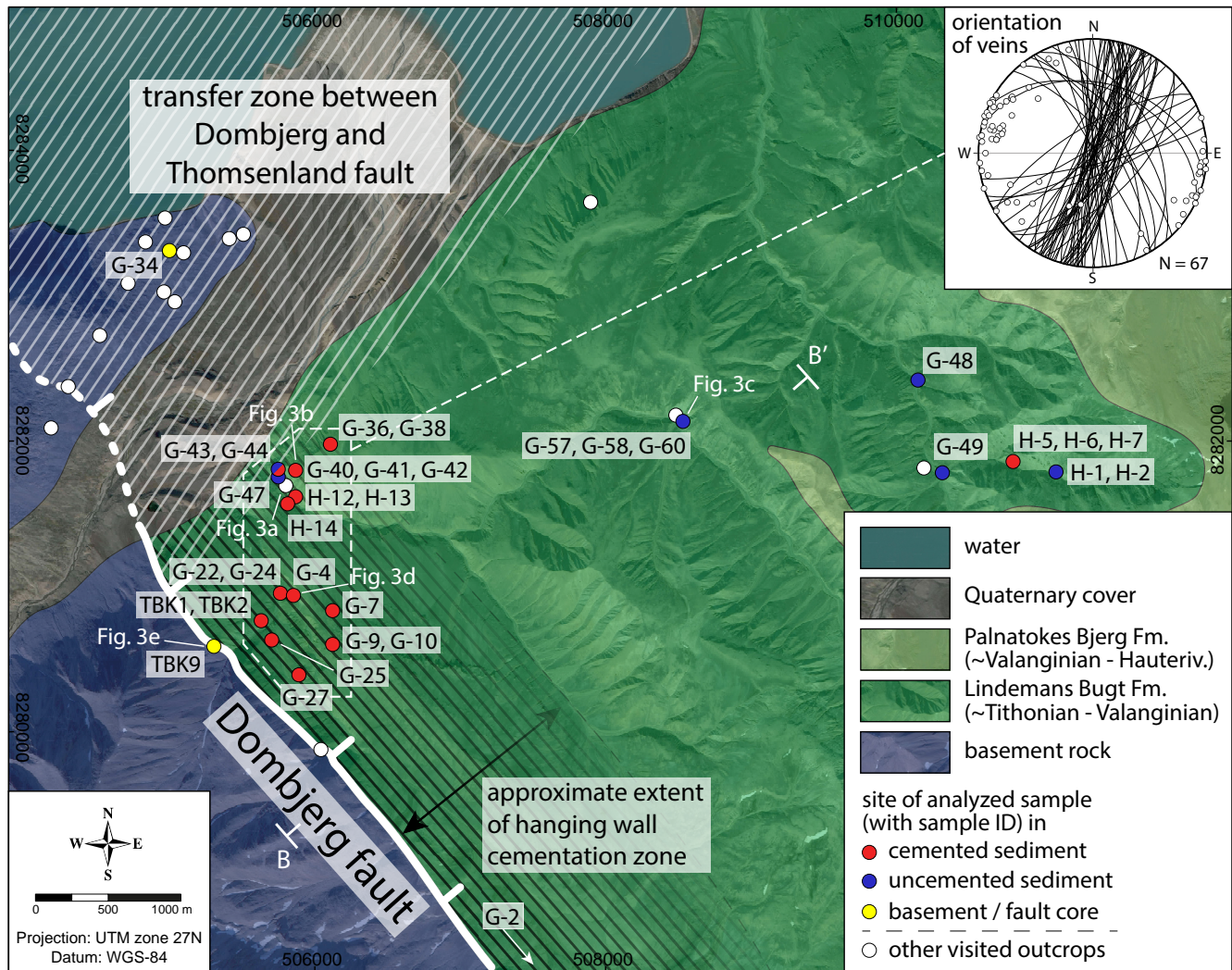


Figure 2. Geological map of study area with locations of visited outcrops and samples analyzed in this study. Inset of stereographic plot shows orientation of all collected calcite veins in the hanging wall. Profile B-B' shown in figure 9-11. Sample coordinates provided in supplementary table S1. See figure 1b for location. Base satellite image from © Google Maps.

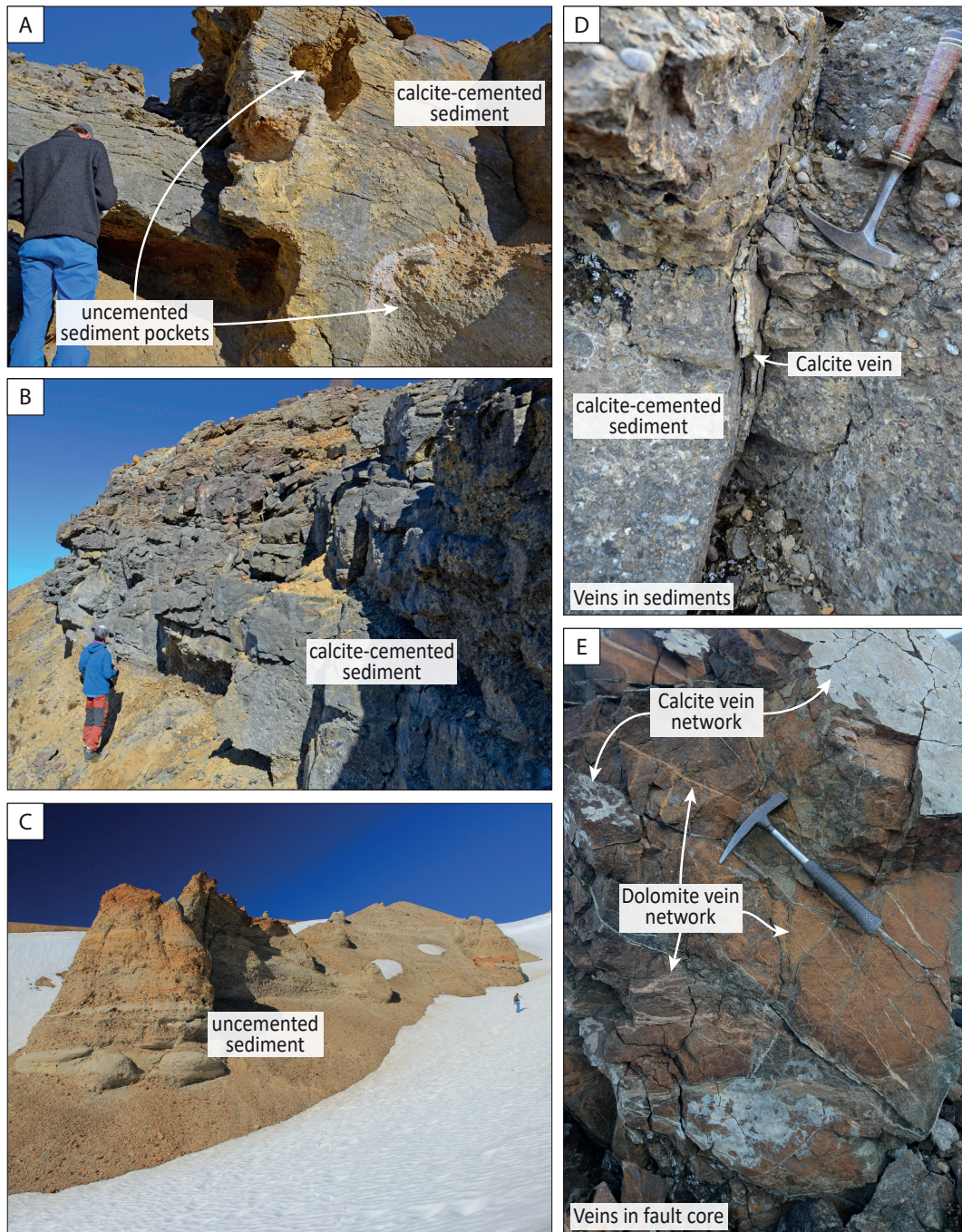


Figure 3. (a) Dolomite-vein-network (yellowish) cut by younger calcite vein-network (whitish) in brecciated basement rock close to Dombjerg Fault core; (b) calcite vein-cutting-through calcite-cemented sandstone within cementation zone; (c) calcite-cemented sandstone with uncemented pockets at the distal end of the cementation zone; (d) calcite cemented conglomerate at distal end of the cementation-chemical alteration zone; (e) uncemented sandstone / conglomerate outside cementation-chemical alteration zone; (f) calcite vein cutting through calcite cemented sandstone within chemical alteration zone; (g) dolomite vein network (yellowish) cut by younger calcite vein network (whitish) within Dombjerg fault core. For location of photos see figure 2.

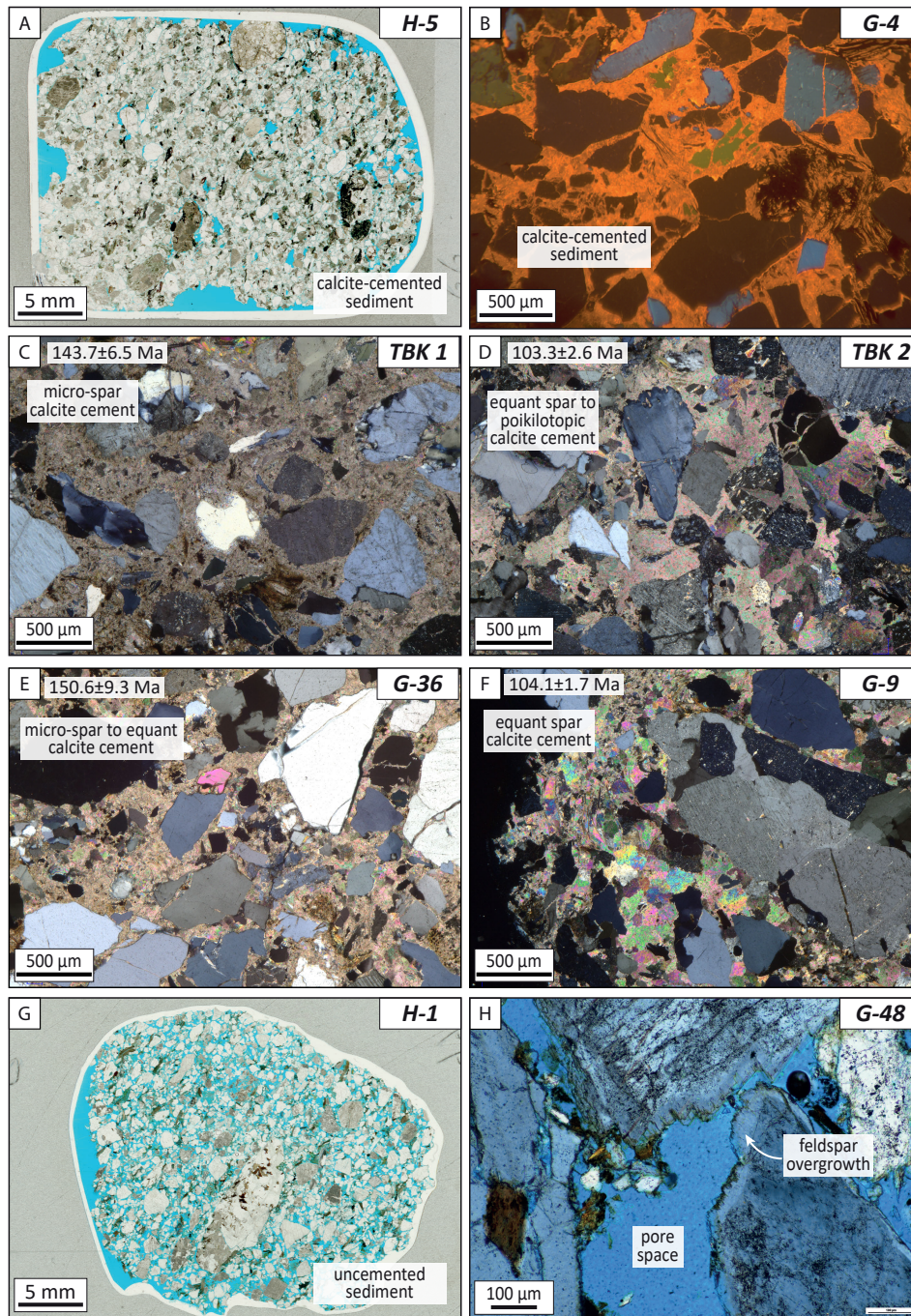


Figure 4. Thin section photos of hanging wall sediments (sample ID in respective upper right corner). (a) Calcite-cemented sample H-5 (plane-polarized light (PPL); oversized pores are caused by plucked grains during sample preparation); (b) close-up cathodoluminescence image of pore-filling drusy calcite spar cement (cross-polarized light (XPL)) calcite-cemented sample; (c-f) close-up of pore-filling poikilotopic calcite cements with textures ranging from micro-spar to poikilotopic cement; (d) cathodoluminescence image of calcite-cemented sample; (e-g) calcite-absent sediment sample H-1 (PPL); (h) close-up of calcite-absent sample with common feldspar-overgrowth (XPL with $\frac{1}{4} \lambda$ plate).

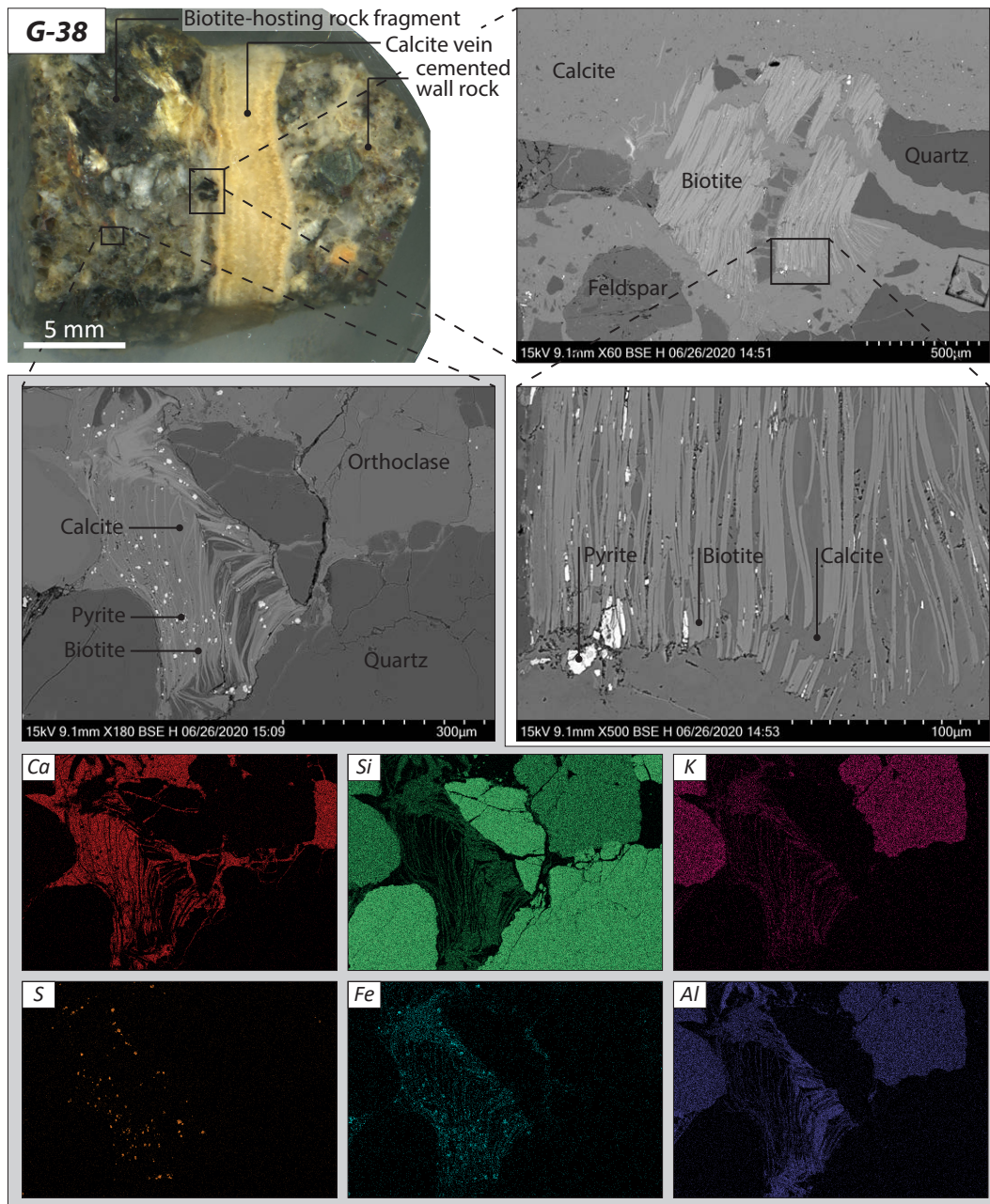


Figure 5. Optical, backscattered-electron, and energy-dispersive X-ray imagery of sample G-38, which hosts abundant biotite in the wall rock. Pyrite is present in the vicinity of biotite grains and between biotite lamellae, which are also pervasively surrounded by calcite.

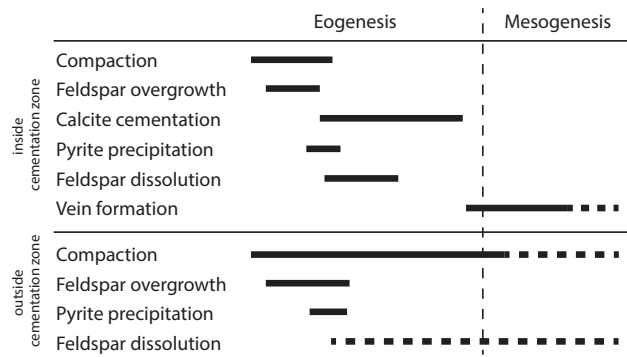


Figure 6. Paragenetic sequence of the main diagenetic events in the Lindemans Bugt Formation.

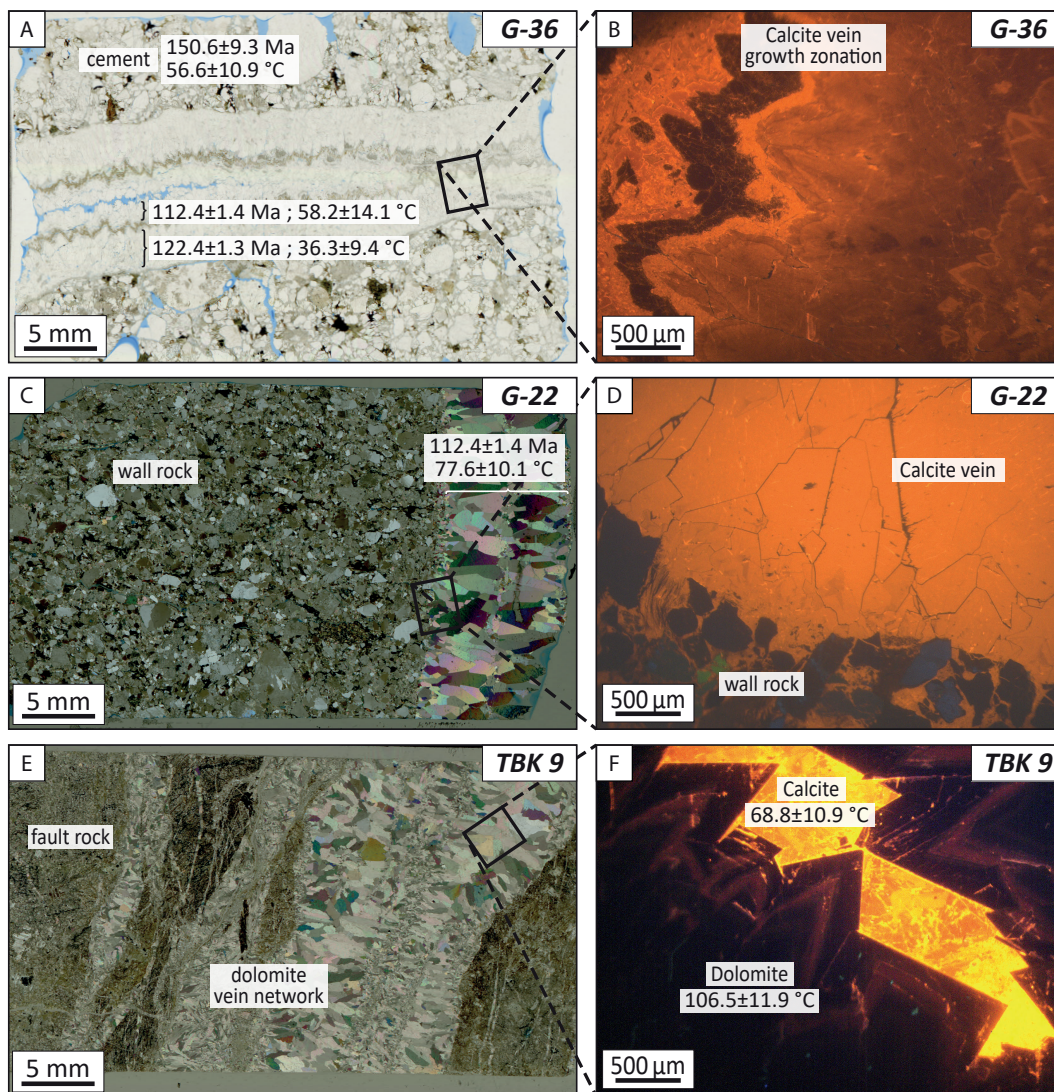
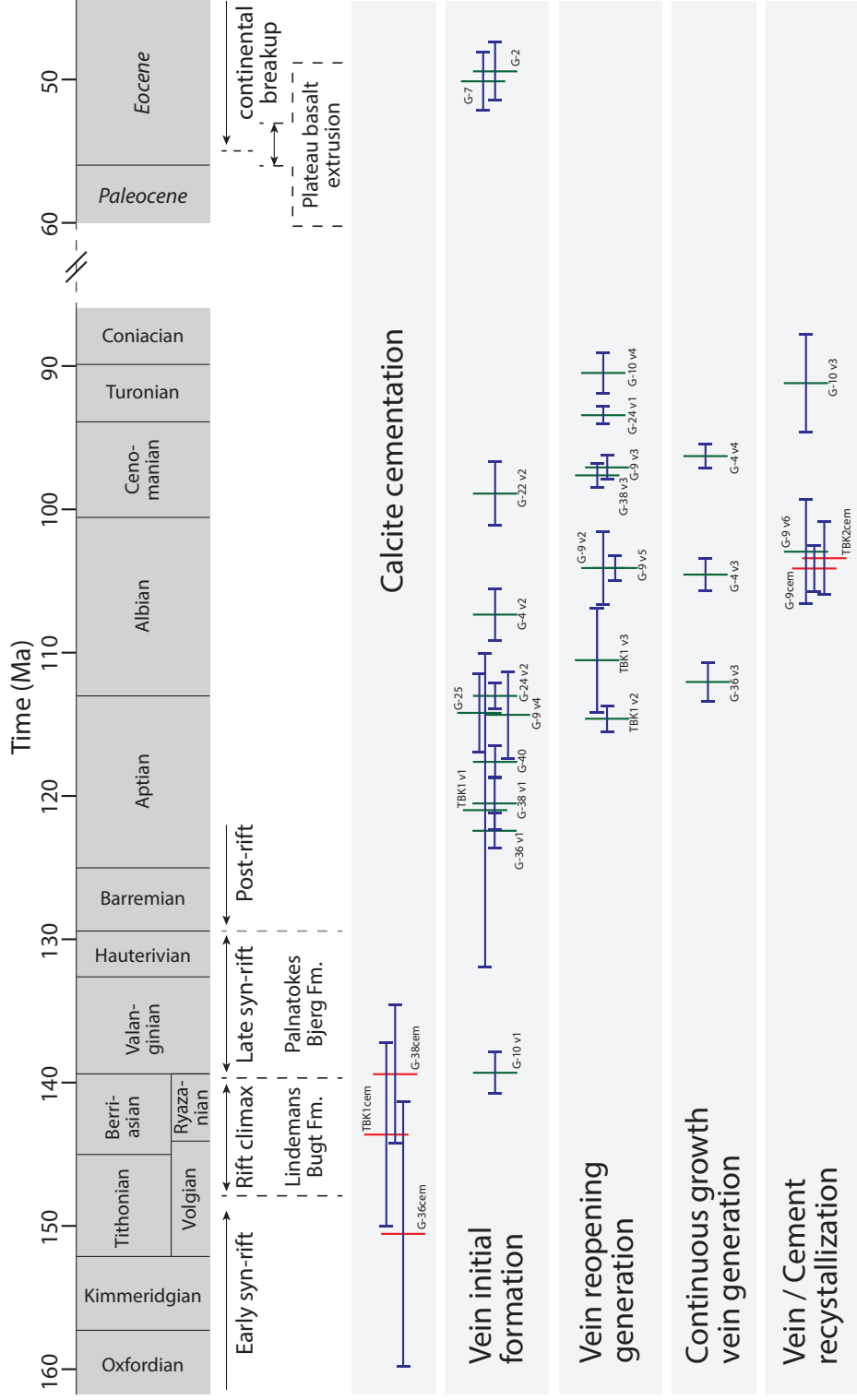


Figure 7. Thin section photos of hanging wall veins (a-d) and fault core veins (e,f). Sample ID given in upper right corner of respective image. Formation ages and temperatures given in figures where available (cf. tables 1, 2). (a) vein showing growth zonation, note ~10 Myr age difference between outer and inner growth generation (plane-polarized light); (b) cathodoluminescence (CL) close-up image of growth zonation; (c) vein devoid of growth zoning (cross-polarized light (XPL)); (d) CL close-up image of calcite vein and calcite-cemented wall rock; (e) dolomite vein network cutting through cataclasite of Dombjerg Fault core (XPL); (f) CL close-up image of dolomite crystals, remaining cavities have been filled with younger calcite.



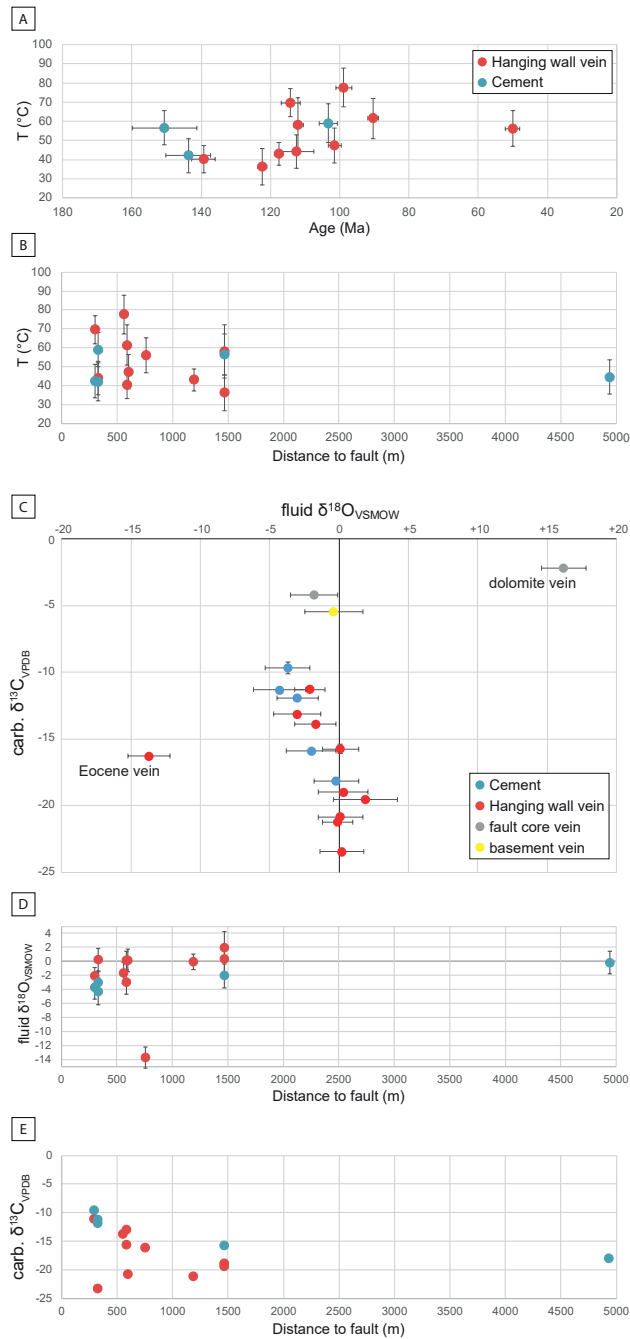


Figure 9. (a) Calcite formation temperatures obtained from clumped isotope analysis against formation ages obtained from U-Pb dating; (b) Calcite formation temperatures against distance to Dombjerg Fault; (c) Fluid $\delta^{18}\text{O}_{\text{VSMOW}}$ against Carbonate $\delta^{13}\text{C}_{\text{VPDB}}$; (d) Fluid $\delta^{18}\text{O}_{\text{VSMOW}}$ against distance to fault; (e) Carbonate $\delta^{13}\text{C}_{\text{VPDB}}$ against distance to fault. (error bars represent 95 % confidence interval)

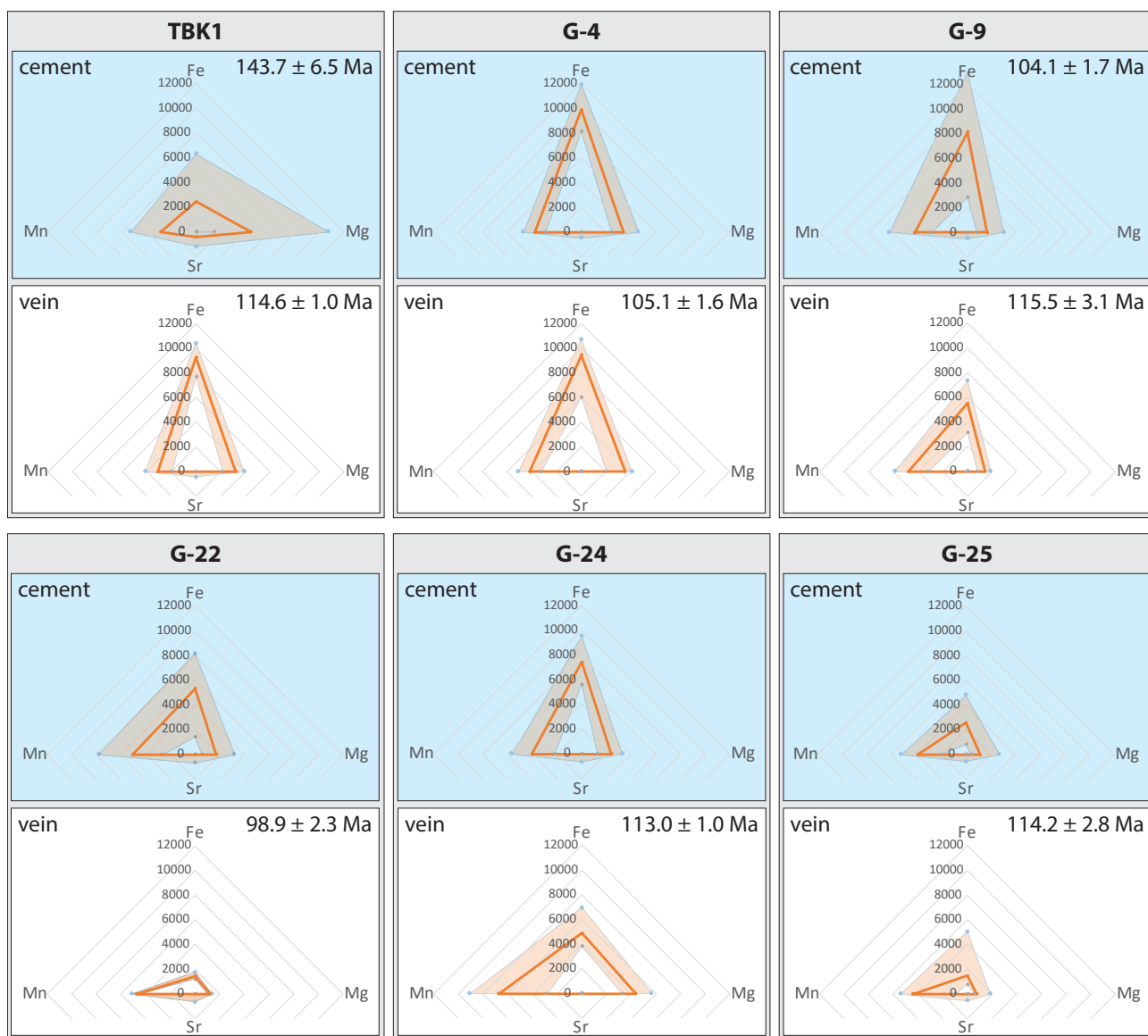


Figure 10. Diagrams showing the element concentrations of Fe, Mn, Mg, Sr (in ppm) in calcite cements and veins. Only samples hosting both cement and veins are shown, and among those samples with multiple vein generations, only data for the thickest vein generation is shown (see supplementary figure S2 for all diagrams). Exceptions are made for Eocene, fault core, and basement samples for which only vein data exist. Solid orange line refers to mean values, the light orange envelope to minimum and maximum values. Note the similarity of element concentration and ratio from cement to vein especially for samples G-4, G-9, G-25, and G-38. The Principal Component Analysis (PCA) plot of the mean values highlights the similar ratio (calculated using provenance R package; Vermeesch et al., 2016).

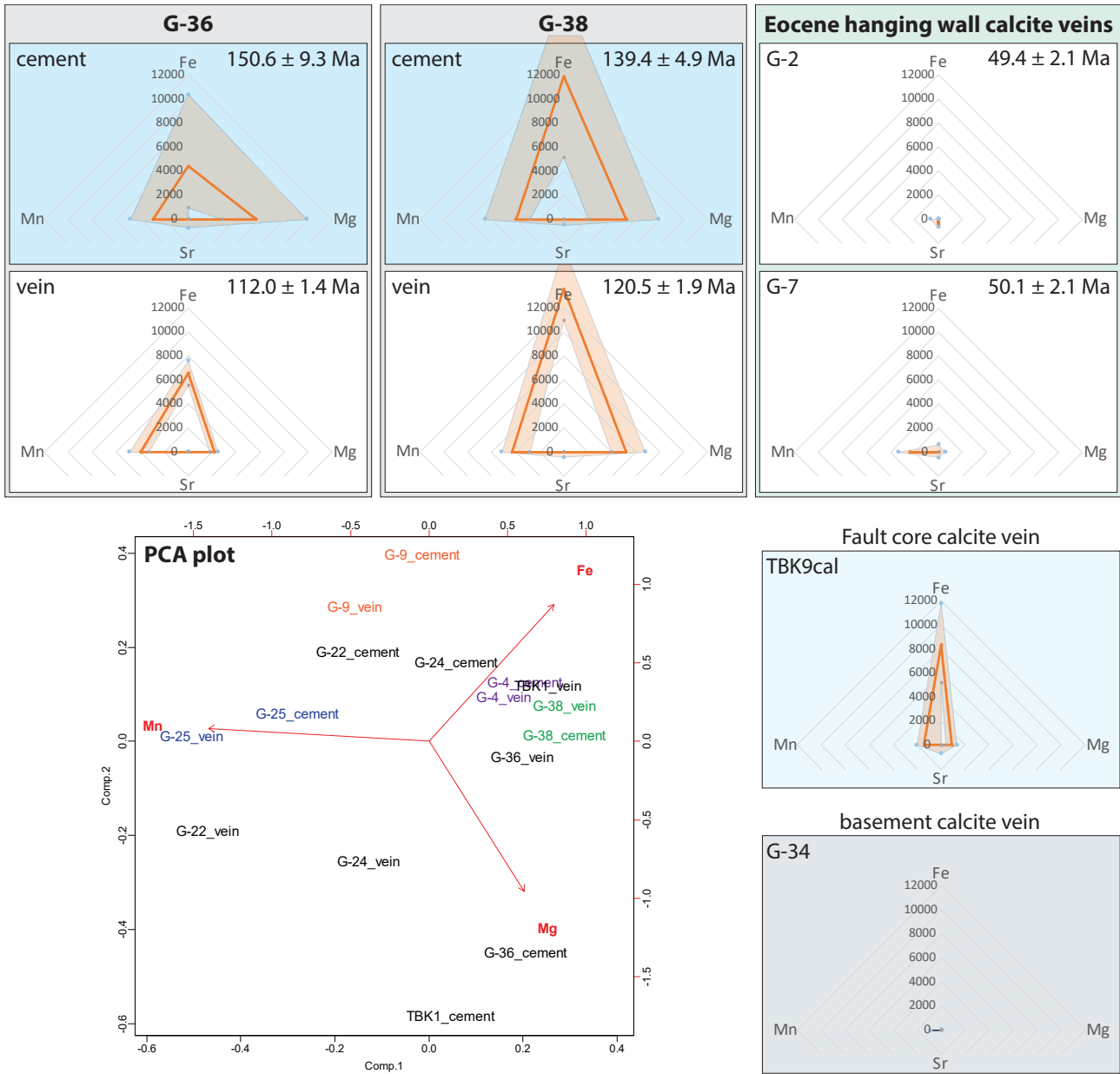


Figure 10. (continued).

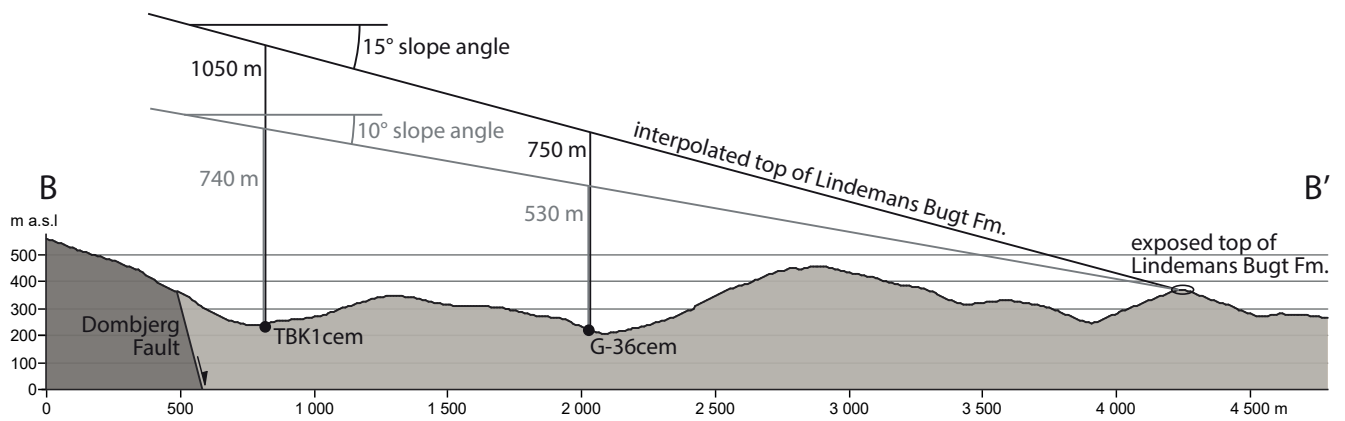


Figure 11. Estimation of thickness of Lindemans Bugt Formation above sample sites. A slope angle of 10-15° is reported for fault-proximal sediments (Henstra et al., 2016) and is used as an interpolation of the top of the formation from its exposure in the field towards the Dombjerg Fault. Sample sites are interpolated onto profile. For location of profile see figure 2.

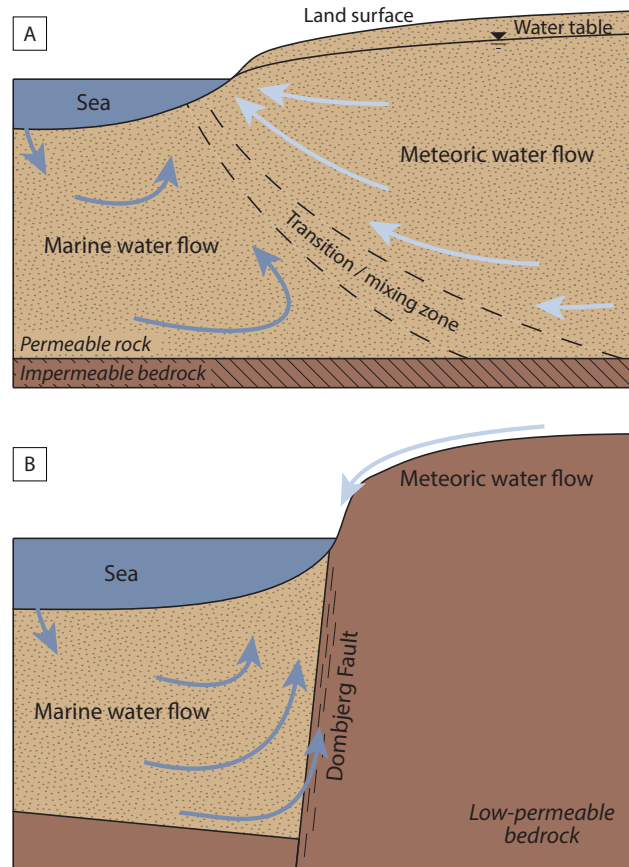


Figure 12. (a) Idealized groundwater flow in coastal areas (redrawn after Jiao and Post, 2019; Cooper et al., 1964). Circulation of saline marine water is tidal-, density-, and thermal-driven. (b) Conceptual adapted fluid flow model at the Dombjerg Fault in the syn-rift stage. Low-permeable footwall rock should cause dominant surficial runoff of meteoric water and circulation of saline-marine water predominantly in the hanging wall and fault zone.

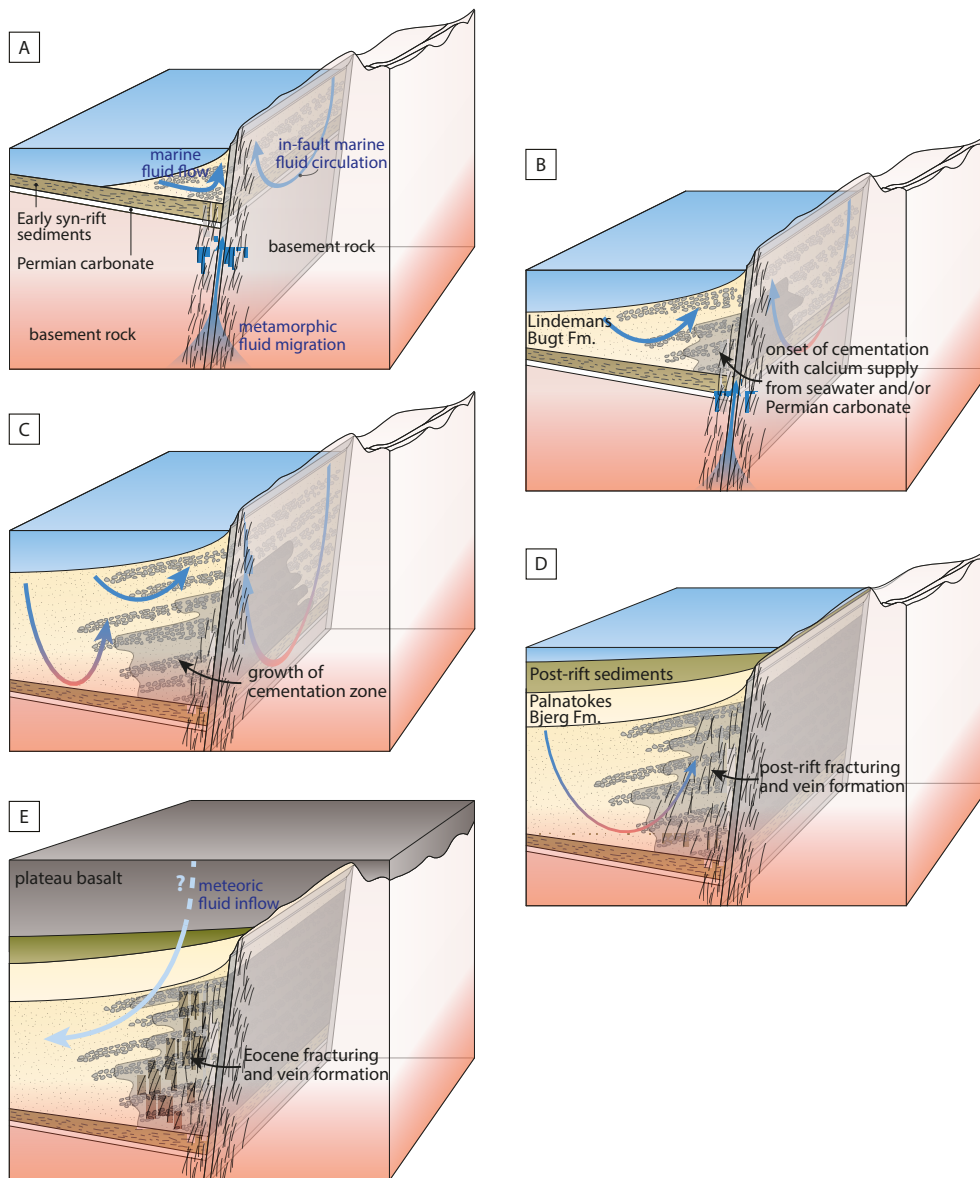


Figure 13. Schematic evolution model of fluid circulation and cementation zone along the Dombjerg Fault. (a) Onset of Dombjerg Fault activity with formation of marine hanging wall basin and syn-rift sedimentation. Circulation of marine fluids is tidal- and thermal-driven (cf. Jiao and Post, 2019). Fault activity maintains a well-connected fracture network in/near the fault core allowing for thermal-driven in-fault circulation of surficial-marine fluids (e.g. López and Smith, 1996) and upward metamorphic fluid migration. (b) Syn-rift sedimentation continues and calcite cement starts to grow. Source of calcium is either seawater or dissolving Permian carbonate underlying syn-rift sediments. (c) Continued syn-rift sedimentation and growth of cementation zone. The zone forms a low-permeable body, which presumably directs thermal-driven marine fluid circulation farther into the basin, which may also allow the cementation zone to grow. (d) Fracturing in the cementation zone occurs mainly in the post-rift stage and vein calcite precipitates from marine fluids. (e) Eocene basalt extrusion and rift shoulder uplift in response to continental breakup drains the marine basin and allows meteoric fluids (pathways unclear) to intrude-infiltrate the hanging wall sediments and Eocene fractures.

Table 1. U-Pb calcite formation ages of calcite cements and veins of the Lindemans Bugt Formation.

Sample	Type	Age $\pm 2\sigma$	MSWD
G-2	initial vein	49.4 \pm 2.1	0.8
G-4 v2	initial vein	107.3 \pm 1.9	0.3
G-4 v3	contin. growth vein	104.5 \pm 1.2	0.7
G-4 v4	contin. growth vein	96.2 \pm 0.9	1.0
G-7 v2	initial vein	50.1 \pm 2.1	1.8
G-9 cem	recryst. cement	104.1 \pm 1.7	2.0
G-9 v4	initial vein	114.4 \pm 3.1	0.7
G-9 v2	reopening vein	104.1 \pm 2.6	1.3
G-9 v3	reopening vein	97.1 \pm 0.9	1.2
G-9 v5	reopening vein	104.1 \pm 0.9	1.4
G-9 v6	recryst. vein	102.9 \pm 3.7	2.1
G-10 v1	initial vein	139.3 \pm 3.4	1.3
G-10 v3	recryst. vein	91.2 \pm 3.5	1.1
G-10 v4	reopening vein	90.4 \pm 1.5	1.0
G-22 v2	initial vein	98.9 \pm 2.3	0.9
G-24 v2	initial vein	113.0 \pm 1.0	1.4
G-24 v1	reopening vein	93.5 \pm 0.7	1.0
G-25	initial vein	114.2 \pm 1.8	1.8
G-36 cem	cement	150.6 \pm 9.3	11.8
G-36 v1	initial vein	122.4 \pm 1.3	0.8
G-36 v3	contin. growth vein	112.0 \pm 1.4	0.7
G-38 cem	cement	139.4 \pm 4.9	5.5
G-38 v1	initial vein	120.5 \pm 1.9	0.1
G-38 v3	reopening vein	97.6 \pm 0.9	0.1
G-40	initial vein	117.6 \pm 1.2	1.4
TBK1 cem	cement	143.7 \pm 6.5	5.8
TBK1 v1	initial vein	121.0 \pm 11.0	2.0
TBK1 v2	reopening vein	114.6 \pm 1.0	1.4
TBK1 v3	reopening vein	110.5 \pm 3.7	1.6
TBK2 cem	recryst. cement	103.3 \pm 2.6	1.8

Table 2. Results from Clumped Isotope Analysis with formation ages from U-Pb dating (cf. table 1). Uncertainties are given at the 95 % confidence interval or as uncertainty propagation (for Fluid $\delta^{18}\text{O}_{\text{VSMOW}}$), n is number of replicates measured of each sample.

type	Samples	Temp (°C)	Fluid $\delta^{18}\text{O}_{\text{VSMOW}}$	Carb. $\delta^{18}\text{O}_{\text{VPDB}}$	Carb. $\delta^{13}\text{C}_{\text{VPDB}}$	Δ_{47}	n	Age (Ma)
cements	TBK1 cem	42.0 ± 10.2	-4.3 ± 1.9	-9.7 ± 0.36	-11.3 ± 0.24	0.619 ± 0.028	14	143.7 ± 6.5
	TBK2 cem	59.0 ± 9.1	-3.0 ± 1.5	-11.3 ± 0.09	-11.9 ± 0.15	0.574 ± 0.022	14	103.3 ± 2.6
	G-25 cem	42.4 ± 8.8	-3.7 ± 1.6	-9.2 ± 0.25	-9.7 ± 0.45	0.618 ± 0.024	14	n/a
	G-36 cem	56.6 ± 10.9	-2.0 ± 1.8	-9.9 ± 0.11	-15.9 ± 0.04	0.580 ± 0.026	14	150.6 ± 9.3
	H-5	44.5 ± 9.0	-0.2 ± 1.6	-6.1 ± 0.05	-18.2 ± 0.21	0.612 ± 0.024	13	n/a
hanging wall veins sorted after distance from fault core	G-25	69.7 ± 7.4	-2.1 ± 1.1	-12.0 ± 0.12	-11.3 ± 0.05	0.549 ± 0.016	13	114.2 ± 2.8
	TBK1	44.1 ± 8.9	+0.2 ± 1.6	-5.6 ± 0.05	-23.5 ± 0.28	0.613 ± 0.024	14	112.5 ± 5.0
	G-10 v1	40.3 ± 7.1	+0.1 ± 1.3	-5.0 ± 0.11	-15.8 ± 0.36	0.624 ± 0.020	14	139.3 ± 3.4
	G-10 v4	61.5 ± 10.5	-3.0 ± 1.7	-11.6 ± 0.07	-13.1 ± 0.04	0.568 ± 0.024	13	90.4 ± 1.5
	G-22	77.6 ± 10.1	-1.7 ± 1.5	-12.8 ± 0.05	-13.9 ± 0.08	0.532 ± 0.020	13	98.9 ± 2.3
	G-4	47.4 ± 9.2	+0.1 ± 1.6	-6.3 ± 0.07	-20.9 ± 0.11	0.604 ± 0.024	13	101.5 ± 1.9
	G-7	55.8 ± 9.2	-13.7 ± 1.5	-21.4 ± 0.12	-16.3 ± 0.14	0.582 ± 0.022	13	50.1 ± 2.1
	G-40	43.1 ± 5.9	-0.1 ± 1.1	-5.7 ± 0.05	-21.2 ± 0.12	0.616 ± 0.016	13	117.6 ± 1.2
	G-36 v3	58.2 ± 14.1	+1.9 ± 2.3	-6.2 ± 0.05	-19.6 ± 0.08	0.576 ± 0.033	13	112.0 ± 1.4
	G-36 v1	36.3 ± 9.4	+0.3 ± 1.8	-4.1 ± 0.09	-19.0 ± 0.16	0.636 ± 0.027	13	122.4 ± 1.3
fault core vein	TBK9cal	68.8 ± 10.9	-1.8 ± 1.7	-11.7 ± 0.05	-4.2 ± 0.07	0.551 ± 0.223	13	n/a
	TBK9dol	106.5 ± 11.9	+16.2 ± 1.6	-15.3 ± 0.33	-2.2 ± 0.12	0.445 ± 0.018	13	n/a
basement vein	G-34	128.7 ± 19.1	-0.4 ± 2.1	-18.0 ± 0.04	-5.5 ± 0.04	0.445 ± 0.025	13	n/a

Table 3. Minor element concentration (in ppm) of calcite cements and veins derived from microprobe analysis (bdl = below detection limit, n = number of measurements).

type	Sample ID	Fe				Mg				n
		Mean	SD	max	min	Mean	SD	max	min	
cements	G-4 cem	9902	121	11929	8138	3424	53	4637	2494	20
	G-9 cem	8116	229	12942	2833	1591	48	2949	756	20
	G-22 cem	5346	180	8187	1411	1736	79	3191	570	20
	G-24 cem	7425	104	9509	5633	2412	55	3291	1287	20
	G-25 cem	2546	107	4789	805	1152	58	2717	435	20
	G-36 cem	4392	223	10353	961	5677	172	9891	2856	20
	G-38 cem	11862	511	18854	5166	5220	178	7906	2073	20
	H-5	6255	48	7160	5532	7557	86	9553	6278	20
	TBK1 cem	2429	239	6307	<i>bdl</i>	4430	304	10727	1496	20
	TBK2 cem	3152	112	5531	1461	1309	47	2979	785	18
Hanging wall veins	G-4 v1	9399	134	10672	6026	3538	60	4124	2036	10
	G-4 v2	8827	63	9590	7432	2857	33	3462	2238	10
	G-4 v3	9356	284	12615	3035	3130	105	4351	971	10
	G-4 v4	6057	105	8396	4219	2401	31	2723	1787	20
	G-40	7323	110	9219	5260	3744	54	4485	2608	10
	G-9 v4	5492	107	7312	3145	1436	28	1902	810	10
	G-9 v5	3829	113	5853	1946	2842	87	3952	711	10
	G-10 v1	6270	219	10021	2077	1581	65	2382	330	20
	G-10 v4	2122	57	3482	1554	401	12	568	<i>bdl</i>	10
	G-22 v1	3126	100	5293	1710	1532	55	2474	851	10
	G-22 v2	1436	22	1744	1188	1204	12	1388	1017	10
	G-24 v1	9636	244	13785	6390	1754	89	3763	821	10
	G-24 v2	4888	90	6937	3826	4381	76	5686	3301	10
	G-24 v3	8245	232	11753	4511	5120	265	7140	545	10
	G-25	1472	131	5015	774	785	40	1855	552	10
	G-36 v3	6567	65	7602	5543	2207	21	2497	1814	10
	G-36 v1	8559	211	13130	5557	4269	108	6453	2753	10
	G-38 v1	13598	216	17041	10964	5180	96	6804	3981	10
	G-38 v3	12860	109	14859	11461	4766	54	5597	4038	10
	TBK1 v1	6563	141	9000	3972	3664	50	4442	2700	20
TBK1 v2	9251	101	10381	7700	3232	61	3897	2175	10	
TBK1 v3	6635	133	8649	4048	2986	78	4303	1734	10	
young veins	G-2	<i>bdl</i>	10							
	G-7	<i>bdl</i>	<i>bdl</i>	604	<i>bdl</i>	<i>bdl</i>	<i>bdl</i>	551	<i>bdl</i>	10
basement / fault core veins	G-34	<i>bdl</i>	10							
	TBK9dol	24556	666	33177	13823	112599	297	116761	109590	10
	TBK9cal	8342	255	11778	5235	887	33	1324	423	10

Table 3. (continued).

type	Sample ID	Sr				Mn				n
		Mean	SD	max	min	Mean	SD	max	min	
cements	G-4 cem	bdl	bdl	493	bdl	3741	46	4663	2882	20
	G-9 cem	bdl	bdl	523	bdl	4277	69	6310	2880	20
	G-22 cem	bdl	bdl	690	bdl	5045	113	7787	2622	20
	G-24 cem	bdl	bdl	671	bdl	4024	79	5647	2189	20
	G-25 cem	bdl	bdl	606	bdl	3895	93	5235	1988	20
	G-36 cem	bdl	bdl	737	bdl	2922	137	4806	bdl	20
	G-38 cem	bdl	bdl	502	bdl	3990	92	6550	2799	20
	H-5	bdl	bdl	554	bdl	4236	34	5039	3844	20
	TBK1 cem	421	26	1224	<i>bdl</i>	2866	137	5291	bdl	20
	TBK2 cem	bdl	bdl	639	bdl	4301	58	5172	3215	18
Hanging wall veins	G-4 v1	bdl	bdl	bdl	bdl	4153	60	5077	3253	10
	G-4 v2	bdl	bdl	508	bdl	4017	36	4468	3283	10
	G-4 v3	bdl	bdl	bdl	bdl	4227	40	5069	3733	10
	G-4 v4	bdl	bdl	846	bdl	5661	85	6256	3315	20
	G-40	bdl	bdl	bdl	bdl	3114	44	3745	2554	10
	G-9 v4	bdl	bdl	bdl	bdl	4795	67	5864	3167	10
	G-9 v5	bdl	bdl	648	bdl	3522	83	4556	1924	10
	G-10 v1	bdl	bdl	453	bdl	4125	91	5714	1979	20
	G-10 v4	bdl	bdl	666	bdl	4043	44	4727	3334	10
	G-22 v1	465	19	705	bdl	5103	148	7700	2720	10
	G-22 v2	bdl	bdl	651	bdl	4745	24	5130	4503	10
	G-24 v1	bdl	bdl	564	bdl	5901	205	8055	2323	10
	G-24 v2	bdl	bdl	bdl	bdl	6719	168	9044	2838	10
	G-24 v3	bdl	bdl	bdl	bdl	5694	145	8926	4106	10
	G-25	bdl	bdl	577	bdl	4387	135	5383	984	10
	G-36 v3	bdl	bdl	bdl	bdl	3959	50	4893	3279	10
	G-36 v1	bdl	bdl	444	bdl	3846	124	6303	2590	10
	G-38 v1	bdl	bdl	448	bdl	4286	89	5153	2823	10
	G-38 v3	bdl	bdl	bdl	bdl	3232	40	3974	2794	10
	TBK1 v1	bdl	bdl	503	bdl	3691	45	4519	2772	20
TBK1 v2	bdl	bdl	429	bdl	3090	57	4120	1955	10	
TBK1 v3	bdl	bdl	464	bdl	2515	50	3152	1403	10	
young veins	G-2	<i>472</i>	<i>14</i>	<i>706</i>	<i>bdl</i>	<i>bdl</i>	<i>bdl</i>	<i>685</i>	<i>bdl</i>	10
	G-7	<i>bdl</i>	<i>bdl</i>	435	<i>bdl</i>	2390	56	3365	1383	10
basement / fault core veins	G-34	<i>bdl</i>	<i>bdl</i>	<i>bdl</i>	<i>bdl</i>	<i>bdl</i>	<i>bdl</i>	862	<i>bdl</i>	10
	TBK9dol	2959	62	4259	2298	1219	46	1722	bdl	10
	TBK9cal	bdl	bdl	695	bdl	1435	44	2012	bdl	10